uOttawa

L'Université canadienne
Canada's university

FACULTÉ DES ÉTUDES SUPÉRIEURES ET POSTOCTORALES

uOttawa

L'Université canadienne
Canada's university

FACULTY OF GRADUATE AND POSDOCTORAL STUDIES

Heather Foucault

AUTEUR DE LA THÈSE / AUTHOR OF THESIS

M.Sc. (Chemistry)

GRADE / DEGREE

Department of Chemistry

FACULTÉ, ÉCOLE, DÉPARTEMENT / FACULTY, SCHOOL, DEPARTMENT

Theoretical and Experimental Investigations of Neutral Ligand Effects in Ruthenium-Mediated Catalysis

TITRE DE LA THÈSE / TITLE OF THESIS

Dr. D. Fogg

DIRECTEUR (DIRECTRICE) DE LA THÈSE / THESIS SUPERVISOR

CO-DIRECTEUR (CO-DIRECTRICE) DE LA THÈSE / THESIS CO-SUPERVISOR

EXAMINATEURS (EXAMINATRICES) DE LA THÈSE / THESIS EXAMINERS

Dr. S. Gambarotta

Dr. D. Richeson

Gary W. Slater

Le Doyen de la Faculté des études supérieures et postdoctorales / Dean of the Faculty of Graduate and Postdoctoral Studies

THEORETICAL AND EXPERIMENTAL INVESTIGATIONS OF NEUTRAL LIGAND EFFECTS IN RUTHENIUM-MEDIATED CATALYSIS

By

HEATHER M. FOUCAULT

Thesis submitted to the
Faculty of Graduate and Postdoctoral Studies
University of Ottawa
In partial fulfillment of the requirements for the degree of

MASTER OF SCIENCE

Ottawa-Carleton Chemistry Institute
University of Ottawa
Ottawa, Ontario
Canada

Your file Votre référence
ISBN: 978-0-494-25771-5
Our file Notre référence
ISBN: 978-0-494-25771-5

ABSTRACT

The activity of novel ruthenium-hydride complexes $RuHCl(CO)(IMes)(PPh_3)$ and $RuHCl(CO)(H_2IMes)(PPh_3)$ was screened for the hydrogenation of sterically-hindered trans internal olefins, and compared to known catalysts $RuHCl(CO)(PCy_3)_2$ and $RuHCl(CO)(IMes)(PCy_3)$. The presence of a labile ancillary donor (i.e. PPh_3) proved to be necessary for the high activity of the *N*-heterocyclic carbene catalysts. However, where possible, competing isomerization and polymerization reactions occurred on the timescale of hydrogenation.

Quantum chemical calculations were performed on model systems $RuHCl(CO)(PH_3)$ and $RuHCl(PH_3)_2$ to identify the role of the carbonyl ligand within the context of catalysis. The resulting data did not support the proposal that this ligand's presence activates the resulting catalyst toward hydrogenation of olefins. No net stabilization of the rate-determining step by CO-containing $RuHCl(CO)(PH_3)_2$ was observed.

The resistance to $\sigma \rightarrow \pi$ isomzerization afforded by a chelating iminopyrrolato ligand was examined through synthesis of $RuCl(\kappa^2\text{-}N,N'\text{-}(2,6\text{-}{}^{i}Pr_2C_6H_3)\text{-}N{=}CHC_4H_3N)(PPh_3)_2]_2$. Retention of the σ-bound binding mode was confirmed on the basis of solution NMR characterization. Data from one dimenional ^{31}P dipolar chemical shift, and two-dimensional ^{31}P-^{31}P *J*-resolved NMR spectra, both of which were gathered in the solid state, confirm that the PPh_3 ligands on each metal center are *cis*-disposed. Data from pulsed field gradient spin echo diffusion NMR experiments establish the dimeric structure of this compound.

TABLE OF CONTENTS

TABLE OF COMPOUND NUMBERS

Number	Compound
1	$RuHCl(CO)(PCy_3)_2$
2	$RuHCl(CO)(IMes)(PCy_3)$
3	$RuHCl(CO)(IMes)(PPh_3)$
4	$RuHCl(CO)(H_2IMes)(PPh_3)$
5	$RuCl_2(PPh_3)_3$
6	2-{(2, 6-^{i}Pr$_2$C$_6$H$_3$)-N=CH}C$_4$H$_4$N
7	Li$^+$[2-{(2, 6-^{i}Pr$_2$C$_6$H$_3$)-N=CH}C$_4$H$_3$N]$^-$
8	$[RuCl(2, 6\text{-}^iPr_2C_6H_3)\text{-}N{=}CHC_4H_3N)(PPh_3)_2]_x$ (**a**: x = 1; **b**: x = 2, PPh_3 ligands are trans; **c**: x = 2, PPh_3 ligands are cis)
9	$RuCl[2\text{-}\{(2, 6\text{-}^iPr_2C_6H_3)\text{-}N{=}CH\}C_4H_3N](CHPh)(L)$ (**a**: L = PCy_3; **b**: L = py)
10	$Ru_2Cl_4(dcypb)_2(N_2)$

LIST OF TABLES

LIST OF SCHEMES

LIST OF FIGURES

LIST OF ABBREVIATIONS

$^{13}C\{^1H\}$	proton-decoupled carbon-13 NMR
$^{31}P\{^1H\}$	proton-decoupled phosphorus-31 NMR
1D	one Dimensional
2D	two Dimensional
Å	Angstrom, 10^{-10} m
atm	atmosphere (1 atm = 760 mmHg, 101.3 kPa, 14.696 psi)
B_0	external magnetic field
BLYP	Becke (exchange), Lee, Yang, Parr (correlation) density functional
B3LYP	Becke 3-Parameter (exchange), Lee, Yang, Parr (correlation) density functional
br	broad
CDA	cyclododecane
CDE	cyclododecene
COE	cyclooctene
COSY	Correlation Spectroscopy
CP	Cross Polarization
CP/MAS	Cross Polarization Magic Angle Spinning
Cy	cyclohexyl
D	diffusion constant, in $m^2\ s^{-1}$
D_C	dipolar coupling, in Hz
d	doublet (NMR)
d_C	residual dipolar coupling, in Hz

dcypb	1,4-bis(dicyclohexylphosphino)butane
DFT	Density Functional Theory
EFG	Electric Field Gradient
EXSY	Exchange Spectroscopy
FID	Free Induction Decay
FT-NMR	Fourier Transform Nuclear Magnetic Resonance
G	gradient strength
ΔG	change in Gibbs free energy, in kJ mol^{-1}
GC	Gas Chromatography
GPC	Gel Permeation Chromatography
H_2IMes	1,3-bis-(2,4,6-trimethylphenyl)imidazolin-2-ylidene
HMBC	Heteronuclear Multiple Bond Coherence
HMQC	Heteronuclear Multiple Quantum Coherence
HOMO	Highest Occupied Molecular Orbital
Hz	Hertz (1 Hz = 1 s^{-1})
I	spin quantum number
I	signal intensity
I_0	signal intensity at zero gradient strength
IMes	1,3-bis-(2,4,6-trimethylphenyl)imidazol-2-ylidene
IR	Infrared
J	spin-spin coupling constant, in Hz
k	Boltzmann's constant, 1.3807×10^{-23} J K^{-1}
L	ligand

m	multiplet (NMR)
m.p.	melting point, in °C
m/z	mass-to-charge ratio
MAS	Magic Angle Spinning
MALDI-TOF	Matrix-Assisted Laser Desorption Ionization Time of Flight
Mes	mesityl
NBD	norbornadiene
NHC	*N*-heterocyclic carbene
NMR	Nuclear Magnetic Resonance
NN′	2-[(2,6-diisopropylphenyl)imino]pyrrolide
PCy_3	tricyclohexylphosphine
PGSE	Pulsed Field Spin Echo spectroscopy
Ph	phenyl
PPh_3	triphenylphosphine
PR_3	tertiary phosphine
ppm	parts-per-million
psi	pounds-per-square-inch (14.696 psi = 1 atm = 760 mmHg, 101.3 kPa)
py	pyridine
pyr	pyrrole
Q	nuclear electric quadrupole moment
r	radius
r_H	hydrodynamic radius
RF	Radio Frequency

ROMP	Ring-Opening Metathesis Polymerization
s	singlet (NMR)
SE	Spin Echo
SECSY	Spin Echo Correlation Spectroscopy
T	Tesla; temperature, in Kelvin (Equation 4.2)
t	triplet (NMR)
T_1	spin-lattice relaxation time constant
T_2	spin-spin relaxation time constant
Tf	triflate
TMS	trimethylsilane
TOF	Turnover Frequency
TS	Transition State
VT-NMR	Variable Temperature Nuclear Magnetic Resonance
XRD	X-Ray Diffraction
Δ	time delay between gradient midpoints
δ	chemical shift, in ppm
δ_G	duration of gradient pulse (Equation 4.1)
δ_{iso}	isotropic chemical shift, in ppm
δ_{11}, δ_{22}, δ_{33}	principal elements of the chemical shift tensor, in ppm
η	descriptor for hapticity; solution viscosity, in N s m^{-2} (Equation 4.2)
γ	gyromagnetic ratio, in T^{-1} s^{-1}
μ	descriptor for bridging
$\nu_{0.5}$	peak width at half height, in Hz

PUBLICATIONS FROM THESIS WORK

- H. M. Foucault, C. N. Rowley, T. Woo, D. E. Fogg, "Computational Investigation of the Activating Effect of CO Ligands in Ruthenium-Catalyzed Hydrogenation" **2007**, manuscript in preparation.

- H. M. Foucault, D. E. Fogg "Transition Metal Catalysts in Organic Synthesis: Ring-Opening Metathesis Polymerization" In *Comprehensive Organometallic Chemistry III* ed.; Crabtree, R. H.; Mingos, M. P., Eds. Elsevier: Oxford, 2007; Vol. 11.

- H. M. Foucault, D. E. Fogg, D. L. Bryce, "A Chelate-Stabilized Ruthenium(σ-Pyrrolato) Complex: Resolving Ambiguities in Nuclearity and Coordination Geometry through ^{1}H PGSE and ^{31}P Solid-State NMR Studies" *Inorganic Chemistry*, **2006**, 45, 10293.

- U. D. Dharmasena, H. M. Foucault, E. N. dos Santos, D. E. Fogg, S. P. Nolan, "N-Heterocyclic Carbenes as Activating Ligands for Hydrogenation and Isomerization of Unactivated Olefins" *Organometallics*, **2005**, 24, 1056.

- S. D. Drouin, H. M. Foucault, G. P. A. Yap, D. E. Fogg, "New Pseudohalide Ligands in Ru-Catalyzed Olefin Metathesis: A Robust, Air-Activated Iminopyrrolato Catalyst" *Can. J. Chem.* (Special Issue in Honour of Howard Alper), **2005**, 83, 748.

ACKNOWLEDGEMENTS

To my supervisor, Dr. Deryn Fogg, I am grateful for your support and guidance these many years. From both a professional and personal perspective, your genuine interest in my development is much appreciated.

I would like to express my sincere thanks to Dr. David Bryce for performing the solid-state NMR experiments in this work and for providing me with every possible opportunity to succeed. Dr. Tom Woo and Christopher Rowley are gratefully acknowledged for their time, effort and insight with respect to the computational calculations. Dr. Glenn Facey, I thank you for your sincere interest in all my work and for making time for me whenever I had a question.

Dr. Jennifer Snelgrove, you were the first person I saw upon my arrival at this university and I thank you for many years of unwavering support and mentorship. I would like to thank Dr. Kenneth Camm for his phenomenal insight, genuine interest and companionship. Jay Conrad, I am grateful for your friendship and am inspired by your innate talent for chemistry. Dr. Melanie Eelman, your constant encouragement and enthusiasm were always appreciated. Sebastien Monfette, for your interest in my work I am truly grateful and it is nice to know that the person who always has my back, has excellent aim. Johanna Blacquiere, your repeated offers of help with this thesis and your friendship are much appreciated. A big thank-you is extended to all my other labmates; including: Renata Cristina Nunes, Joao Duarte Silva, Pawel Czechura, Nicholas Beach and Ureshini Dharmasena for many interesting conversations.

To the people in my life that I love, I owe you everything.

"I don't like work, no one does, but I, like what is in the work, the chance to find yourself."
from Heart of Darkness by Joseph Conrad

CHAPTER 1

Introduction

1.1. Homogeneous Catalysis

Catalytic processes are relevant to every area of chemical synthesis; they account for over 85 % of all reactions and represent the most efficient and environmentally-friendly route to many industrially-relevant compounds.[1] Commercially, this field is dominated by heterogeneous systems, which are definitely more economical than homogeneous (molecular) catalysts. However, heterogeneous systems are ill-defined at the molecular level.[2] Homogeneous catalysts are well-defined, and thus more selective, but suffer from issues relating to longevity and separation of product from catalyst solution.[2] As a compensating advantage these systems can, in principle, be characterized completely by spectroscopic techniques, and possess reaction kinetics that can be equally related to each active metal atom.[3] This permits a more detailed mechanistic understanding than is afforded by the heterogeneous systems. The consequence of this is that homogeneous catalysts can be tailor-made for highly specialized reactions, offering the greatest possible degree of regio-, chemo- and enantioselectivity.

1.2. Homogeneous Hydrogenation

Dihydrogen is the simplest molecule, and the cleanest and most abundant reducing agent. The impact of reactions with molecular hydrogen are far-reaching; addition of H_2 is relevant to both the large-scale production of saturated compounds, and to the development of fine chemicals for highly-specialized applications.[3-5] Hydrogenation of unsaturated bonds is also a known method for protecting materials from oxidative and thermal degradative pathways.[6,7]

Under ambient conditions, however, molecular hydrogen is unreactive[8] and hydrogenation is always preceded by initial activation of H_2 by a metal catalyst.

1.2.1. Mechanistic Overview

Addition of H_2 across an unsaturated bond is thermodynamically favourable but symmetry forbidden in the ground state.[9] In a concerted *cis* addition (Figure 1.1), electrons cannot flow from the filled σ-orbital on H_2 to the unfilled π*-orbital on the olefin because there is no net orbital overlap. Transition metal *d*-orbitals, however, posses the correct symmetry to interact with H_2 directly; a filled metal *d*-orbital overlaps with the empty H_2 σ*-orbital and causes dissociation of the H-H bond. The products of this transformation are two metal-hydride bonds of the correct symmetry to permit transfer of a hydrogen atom to an olefin.

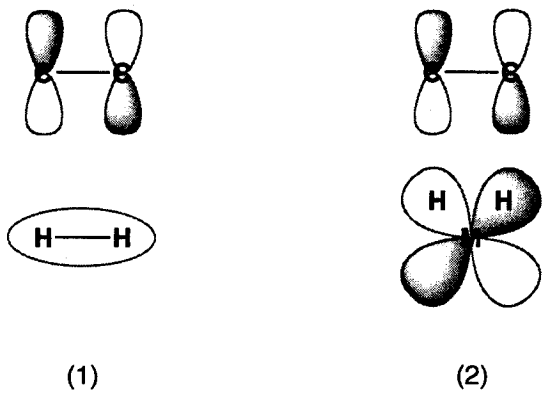

Figure 1.1 Symmetry-forbidden addition of H_2 to a carbon-carbon double bond (1) and metal-catalyzed allowed concerted addition of two H atoms across a carbon-carbon double bond (2).

For many transition metal hydrogenation catalysts, activation of H_2 occurs via an inner sphere mechanism (i.e. H_2 interacts with the metal centre directly). This activation can occur by either oxidative addition or heterolytic splitting of H_2. Dihydrogen activation by an oxidative

addition occurs via a three-centered, two-electron transition state, and is most favoured for square planar d^8 metal complexes; addition results in formation of a octahedral d^6 metal centre.[8] The first well-defined species to exhibit activation by this method was Wilkinson's catalyst, $RhCl(PPh_3)_3$. Molecular hydrogen adds to $RhCl(PPh_3)_3$, formation of two hydrides labilizes one of the PPh_3 ligands, and a vacant site is then created for olefin coordination (Scheme 1.1).[10] The intermediate alkyl generated following olefin coordination and insertion of the olefin into the metal-hydride bond, then undergoes reductive elimination with the second hydride to generate an alkane. A dissociative mechanism, in which PPh_3 is lost first, is favoured for reactions mediated by catalysts with at least one of the following: an overall positive charge on the metal or an environment of low free phosphine concentration. This pathway, where $RhCl(PPh_3)_2$ reacts with H_2, is 10^4 times faster than the analogous reaction with $RhCl(PPh_3)_3$.[11,12] For both the dissociative and hydridic possibilities, kinetic[13] and computational analysis at the *ab initio*[14] and B3LYP[15] levels of theory suggest that olefin insertion into the Rh-H bond is the rate-determining step, and that the overall reaction is exothermic.

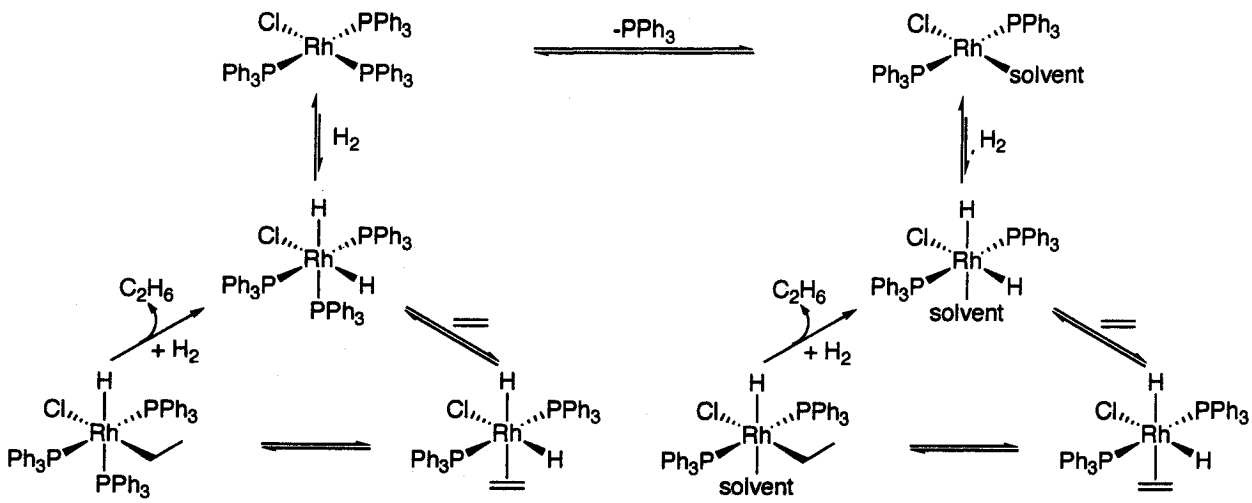

Scheme 1.1 Associative and dissociative mechanisms for olefin hydrogenation by Wilkinson's catalyst. The right-hand mechanism (dissociative) is dominant.

Ruthenium hydrogenation catalysts activate H_2 by either oxidative addition or net heterolysis.[16] Kinetic studies[17,18] indicate that the mechanism for hydrogenation is dissociative, for phosphine-containing catalysts, and that the active catalyst is generated by initial phosphine loss. Olefin coordination to the active catalyst results in formation of a π-bound olefin complex that rearranges to a σ-alkyl complex by insertion of the olefin into the metal-hydride bond. Coordination of H_2 results in formation of a Ru-H_2 complex. The increase in acidity of the protons of the H_2 ligand enables deprotonation by the alkyl ligand and the active catalyst is regenerated when the saturated product is eliminated.[19] This last step is fast and irreversible (Scheme 1.2). By heterolytically activating H_2 and avoiding oxidative addition, formation of a Ru(IV) intermediate is bypassed, which can be an unstable oxidation state for ruthenium.[2] Some of these reported Ru(IV) complexes represent transient species where the equilibrium lies more in favour of the corresponding dihydride-hydrogen complex $Ru(H)_2(H_2)$ instead.

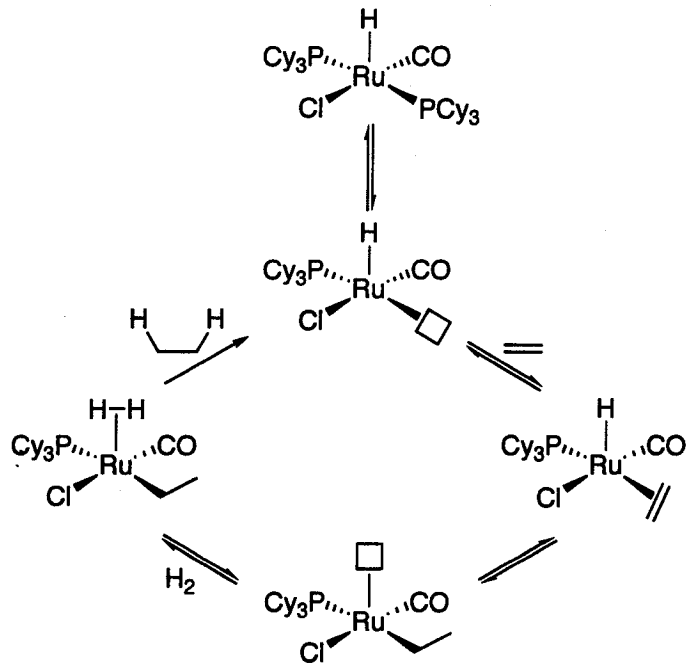

Scheme 1.2 Mechanism for olefin hydrogenation by benchmark $RuHCl(CO)(PCy_3)_2$.

Kinetic studies indicate that the rate-determining step for Ru-catalyzed hydrogenation is olefin insertion into the Ru-H bond, paralleling the analogous Rh-catalyzed reaction. The only computational confirmation of this finding has been through analysis of the reduction of norbornadiene (NBD) by $RuH(OTf)(NBD)(PPh_3)_2$ at the BLYP level of density functional theory.[20] A similar analysis of the common catalyst architecture $RuHCl(X)(L)_2$ does not exist. However, key advances have been made into the understanding of the proposed reaction intermediates, including the Ru-H_2 complex[21] and olefin insertion into the Ru-H bond.[22-24]

1.2.2. Neutral Ligand Effects in Homogeneous Hydrogenation

1.2.2.1. The Carbon Monoxide Ligand in Transition Metal Hydrogenation Catalysts

Incorporation of π-acidic species has mixed effects on the rate of hydrogenation, depending on the transition metal mediating the catalysis. Rhodium and iridium carbonyl complexes, for example, are less active than their non CO-containing complexes.[18] These metals activate H_2 by oxidative addition.[8] Incorporation of strongly π-acidic species promotes η^2–coordination of dihydrogen rather than dissociation through stabilization of the metal *d*-orbitals by back donation. The required high-spin d^6-configuration needed for donation into the H-H σ^*–orbital, to create the dihydride, is not energetically favourable (Figure 1.2).[22,25]

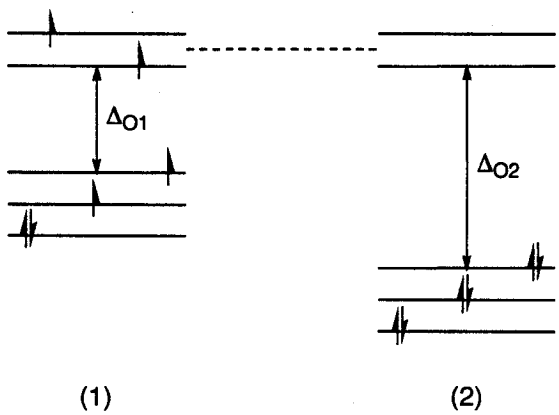

Figure 1.2 Orbital diagram of metal *d*-orbitals representing a high-spin d^6 configuration (1) and a low-spin d^6 configuration (2). The HOMOs in (2) are stabilized by back-donation from CO.

The incorporation of a carbonyl ligand into hydrido ruthenium catalysts containing alkylphosphines can result in enhanced hydrogenation activity. This effect is readily observed in tandem catalytic processes, where Ru-alkylidenes are transformed into olefin reduction catalysts in the presence of an alcohol co-solvent and a base. Known hydrogenation catalyst $RuHCl(CO)(PCy_3)_2$ is generated in situ from reaction of Grubbs-type catalysts

($RuCl_2(CHPh)(LL')$) with methanol in the presence of triethylamine (Scheme 1.3).[26,27] The decarbonylation of methanol by Ru(II) complexes is well established in the literature,[28] and may account for the increased hydrogenation activities reported this solvent.[29]

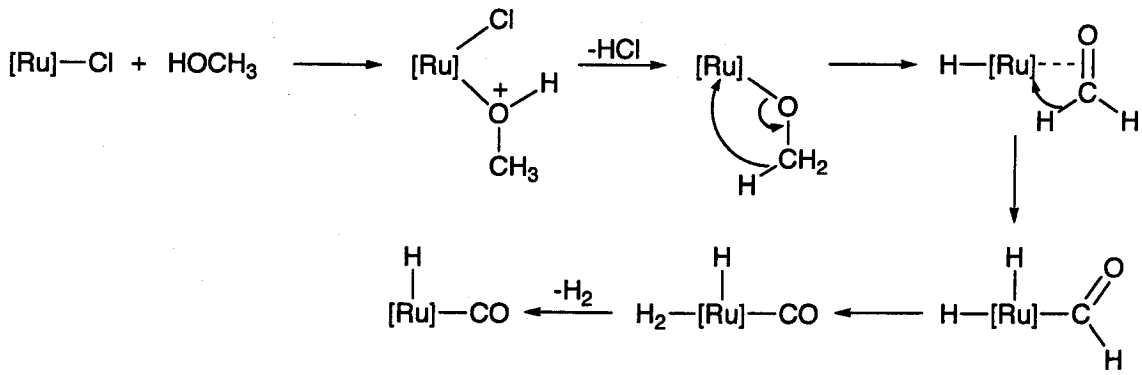

Scheme 1.3 The decarbonylation of methanol by a Ru(II) compound ([Ru] = $RuCl(PPh_3)_3$).

However, the role of the carbonyl ligand in catalysis is not well understood. Heterolytic activation of H_2, prior to reductive elimination of the saturated product, may result in a ruthenium dihydride where the metal exists in a transient +4 oxidation state. The observation of $Ru(H)_2Cl_2(PCy_3)_2$ may be possible indirect evidence for this theory.[30] Addition of a π-acidic ligand would tend to destabilize the Ru(IV) complex via back-donation of electron density from the metal to the π^* orbitals on the ligand. This effect would decrease the barrier for reductive elimination of the saturated product. Heterolytic activation also implies donation of electron density from the H-H σ-orbital, which would be favoured by the stabilization of metal *d*-orbitals by CO.

1.2.2.2. *N*-Heterocyclic Carbenes as Ligands in Transition Metal Hydrogenation Catalysts

Wanzlick and Ofele first reported the use of *N*-heterocyclic carbenes as ligands for transition metal compounds almost 40 years ago.[31,32] Their widespread use as ligands was not practical until the isolation of the first free carbene by Arduengo and co-workers more than 20 years later.[33] *N*-heterocyclic carbenes, when bound to a metal, are less reactive than both Fischer and Schrock carbenes (Figure 1.3) but they still participate in side-reactions with the metal centre. These side reactions include ortho-metallation and reductive elimination.[34]

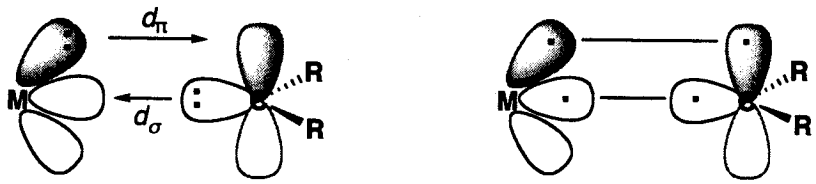

(1) (2)

Figure 1.3 Fischer (1) and Schrock (2) carbene classes.

Initially, an analogy was drawn between *N*-heterocyclic carbenes and phosphines: both ligand classes are neutral, two electron almost σ-donors with poor π-acceptor capabilities.[35] Further study showed these two ligand classes to be more distinct. *N*-heterocyclic carbenes are more basic (better σ-donors) than the most basic phosphines[36-38] and their two-dimensional steric demand, relative to the cone shape of PR_3, permits the incorporation of larger side-groups. Incorporation of *N*-heterocyclic carbenes as phosphine replacements has been linked directly to enhanced activity for many catalytic processes, including olefin metathesis,[36,39] and hydrogenation [40-46] and isomerization.[45-47] With respect to olefin hydrogenation, however, *N*-heterocyclic carbene-containing systems have enjoyed less success, and until recently, have been useful only at high temperatures and pressures.[46]

1.3. Bimolecular Deactivation of Chlororuthenium Olefin Metathesis Catalysts

Olefin metathesis has emerged as a powerful tool for the synthesis of structurally diverse organic and polymeric materials.[48] While a range of well-defined catalysts for this transformation exist, integration of selectivity (regio-, chemo-, enantio-), reactivity and robustness remains elusive. The Schrock and Grubbs class of olefin metathesis catalysts have had the most significant impact in this regard. Schrock catalysts are high oxidation state molybdenum-alkylidene complexes that accommodate a wide range of aryloxide, alkoxide and imido functional groups. These catalysts are among the most selective for asymmetric ring-closing metathesis and ring-opening metathesis polymerization[49,50] but are very sensitive to air, water and polar functional groups. While the first generation Grubbs catalyst ($RuCl_2(CHPh)(PCy_3)_2$) lagged in lifetime and activity, relative to the Schrock catalysts, superior functional group tolerance and robustness was achieved. Incorporation of *N*-heterocyclic carbenes,[36, 51-53] labile neutral ligands (i.e. PPh_3,[36] pyridine[54, 55]) and activated styrenyl ethers[56-58] made Ru-catalysts competitive with the Mo systems.

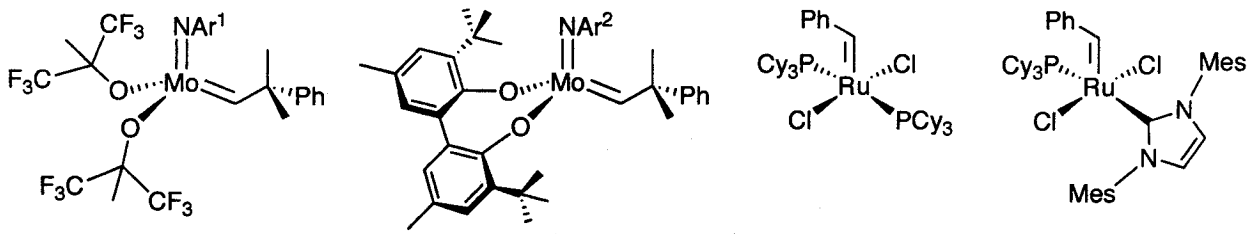

Figure 1.4 Selected olefin metathesis catalysts (from left): Schrock catalyst (Ar^1 = 2,6-$^i Pr_2$-C_6H_3),[59] asymmetric Schrock catalyst (Ar^2 = 2,6-Me_2-C_6H_3),[60] Grubbs first generation catalyst,[61] second generation catalyst.[36]

Work by the Fogg group showed that decomposition of the Grubbs-class of catalysts is promoted by the presence of chloride ligands, which enable a bimolecular decomposition

pathway (Scheme 1.4).[62] Since this finding, *N*-heterocyclic carbene complexes have also been implicated in a bimolecular decomposition pathway.[63] In an attempt to circumvent the former transformation, formation of a $Ru_2(\mu\text{–}Cl)_3$ dimer, the chloride ligands were replaced by alternative anionic donors or 'pseudohalide' ligands.

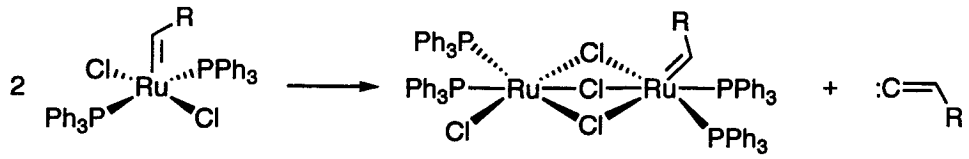

Scheme 1.4 Bimolecular decomposition of a Grubbs-type catalyst.[64]

Incorporation of aryloxide ligands into the Grubbs-type catalysts has promoted increases in catalyst lifetime.[65, 66, 67] A complicating factor inherent in the use of aryloxides is their tendency for $\sigma \rightarrow \pi$ isomerization, generating catalytically-inactive piano stool complexes. The Fogg group has noted previously the ease with which phenoxide undergoes this transformation in systems containing labile ancillary ligands.[68,69] One solution to this problem is the incorporation of electron-deficient aryloxides, such as perfluorophenoxide, where π-donor ability is significantly reduced.[70] Incorporation of a chelating pseudohalide is also a possibility, and $\sigma \rightarrow \pi$ isomerization would be prevented by the thermodynamic stability of the chelate ring.[71, 72]

1.4. Scope of Thesis Work

This thesis is directed at clarifying fundamental concepts relating to the structure and bonding in ruthenium catalysts for olefin hydrogenation and metathesis. Ultimately, this work is directed at the improvement of existing species. Experimental procedures are discussed in Chapter 2. Chapter 3 describes a computational investigation of the behaviour of π-acidic ligands, namely carbon monoxide, in ruthenium-catalyzed hydrogenation. Olefin reductions mediated by ruthenium hydridocarbonyl species containing *N*-heterocyclic carbenes are also investigated, with emphasis being placed on their activity in the presence of a highly labile ancillary donor. The potential of pyrrolide derivatives as N-based pseudohalide ligands is explored in Chapter 4, in which the synthesis of a chelate-stabilized ruthenium (σ-pyrrolato) complex is discussed Finally, general conclusions and recommendations for future work are provided in Chapter 5.

1.5 References

(1) Parshall, G. W.; Ittel, S. D., *Homogeneous Catalysis.* 2nd ed.; Wiley-Interscience: Toronto, 1992; p 342.

(2) Crabtree, R. H., *The Organometallic Chemistry of the Transition Metals.* 3rd ed.; Wiley-Interscience: Toronto, 1994.

(3) Cornils, B.; Herrmann, W. A., *J. Catal.*, **2003**, *216*, 23.

(4) Blaser, H.-U.; Malan, C.; Pugin, B.; Spindler, F.; Steiner, H.; Studer, M., *Adv. Synth. Catal,* **2003**, *345*, 103.

(5) Noyori, R., *Angew. Chem. Int. Ed.*, **2002**, *41*, 2008.

(6) (a) McLain, S. J.; McCord, E. F.; Arthur, S. D.; Hauptman, E.; Feldman, J.; Nugent, W. A.; Johnson, L. K.; Mecking, S.; Brookhart, M. *Proc. PMSE* **1997**, *76*, 246. (b) Dias, E. L.; Grubbs, R. H. *Organometallics* **1998**, *17*, 2758. (d) Bielawski, C. W.; Louie, J.; Grubbs, R. H. *J. Am. Chem. Soc.*, **2000**, *122*, 12872.

(7) Barrett, A. G. M.; Hopkins, B. T.; Koebberling, J., *Chem. Rev.*, **2002**, *102*, 3301.

(8) James, B. R., Comprehensive Organometallic Chemistry. In *Comprehensive Organometallic Chemistry*, Wilkinson, G., Ed. Pergamon Press: New York, 1982; Vol. 8, Chapter 51, and references therein.

(9) Pearson, R. G., *Acc. Chem. Res,* **1971**, *4*, 152.

(10) Chaloner, P. A.; Esteruelas, M. A.; Joo, F.; Oro, L. A., *Homogeneous Hydrogenation.* Kluwer: Boston, 1994.

(11) Halpern, J.; Wong, C. S., *J. Chem. Soc., Chem. Commun.*, **1973**, 629.

(12) Tolman, C. A.; Meakin, P. Z.; Lindner, D. I.; Jesson, J. P., *J. Am. Chem. Soc.*, **1974**, *96*, 2762.

(13) Candlin, J. P.; Oldham, A. R., *Faraday Discuss.*, **1968**, *46*, 60.

(14) Daniel, C.; Koga, N.; Han, J.; Fu, X. Y.; Morokuma, K., *J. Am. Chem. Soc.*, **1988**, *110*, 3773.

(15) Luo, X.; Tang, D.; Li, M., *THEOCHEM*, **2005**, *714*, 179.

(16) Clapham, S. E.; Hadzovic, A.; Morris, R. H., *Coord. Chem. Rev.*, **2004**, *248*, 2201.

(17) Hallman, P. S.; McGarvey, B. R.; Wilkinson, G., *J. Chem. Soc. A*, **1968**, 3143.

(18) James, B. R., *Homogeneous Hydrogenation*. John Wiley & Sons: Toronto, 1973; p. 525 and references therein.

(19) Crabtree, R. H.; Hamilton, D. G., *J. Am. Chem. Soc.*, **1986**, *108*, 3124.

(20) Lo, S. T.; Xu, Z.; Wen, T. B.; Ng, W. S.; Liu, S. H.; Zhou, Z. Y.; Lin, Z.; Lau, C. P.; Jia, G., *Organometallics*, **2000**, *19*, 4523.

(21) Maseras, F.; Lledos, A.; Clot, E.; Eisenstein, O., *Chem. Rev.*, **2000**, *100*, 601.

(22) Niu, S.; Hall, M. B., *Chem. Rev.*, **2000**, *100*, 353.

(23) Gerard, H.; Eisenstein, O., *J. Chem. Soc., Dalton Trans.*, **2003**, 839.

(24) Marchenko, A. V.; Gerard, H.; Eisenstein, O.; Caulton, K. G., *New. J. Chem.*, **2001**, *25*, 1382.

(25) Hay, P. J., *J. Am. Chem. Soc.*, **1987**, *109*, 705.

(26) Drouin, S. D.; Zamanian, F.; Fogg, D. E., *Organometallics*, **2001**, *20*, 5495.

(27) Drouin, S. D.; Yap, G. P. A.; Fogg, D. E., *Inorg. Chem.*, **2000**, *39*, 5412.

(28) (a) Chen, Y.; Chan, W. C.; Lau, C. P.; Chu, H. S.; Lee, H. L.; Jia, G. *Organometallics*, **1997**, *16*, 1241. (b) Coalter, J. N.; Huffman, J. C.; Caulton, K. G. *Organometallics*, **2000**, *19*, 3569. (c) Marchenko, A. V.; Huffman, J. C.; Valerga, P.; Tenorio, M. J.; Puerta, M. C.; Caulton, K. G. *Inorg. Chem.*, **2001**, *40*, 6444. (d) Chaudret B. N.; Cole-Hamilton, D. J.; Nohr, R. S.; Wilkinson, G. *J. Chem. Soc., Dalton Trans.*, **1977**, 1546. (e) Van Der Sluys, L. S.; Kubas, G. J.; Caulton, K. G. *Organometallics*, **1991**, *10*, 1033.

(29) (a) Nkosi, B. S.; Coville, H. J.; Albers, M. O.; Gordon, C.; Viney, M.; Singleton, E. *J. Organomet. Chem.* **1990**, *386*, 111. (b) Fogg, D. E.; James, B. R.; Kilner, M. *Inorg. Chim. Acta* **1994**, *222*, 85. (c) Zanetti, N. C.; Spindler, F.; Spencer, J.; Togni, A.; Rihs, G. *Organometallics* **1996**, *15*, 860. (d) Bianchini, C.; Barbaro, P.; Scapacci, G.; Zanobini, F. *Organometallics* **2000**, *19*, 2450.

(30) Rodriguez, V.; Sabo-Etienne, S.; Chaudret, B.; Thoburn, J.; Ulrich, S.; Limbach, H.-H.; Eckert, J.; Barthelat, J.-C.; Hussein, K.; Marsden, C. J., *Inorg. Chem.*, **1998**, *37*, 3475.

(31) Oefele, K., *J. Organomet. Chem.*, **1968**, *12*, 42.

(32) Wanzlick, H. W.; Schoenherr, H. J., *Angew. Chem. Int. Ed.*, **1968**, *7*, 141.

(33) Arduengo, A. J.; Harlow, R. L.; Kline, M., *J. Am. Chem. Soc.*, **1991**, *113*, 361.

(34) Crudden, C. M.; Allen, D. P., *Coord. Chem. Rev.*, **2004**, *248*, 2247.

(35) Peris, E.; Crabtree, R. H., *Coord. Chem. Rev.*, **2004**, *248*, 2239.

(36) Huang, J.; Stevens, E. D.; Nolan, S. P.; Petersen, J. L., *J. Am. Chem. Soc.*, **1999**, *121*, 2674.

(37) Perrin, L.; Clot, E.; Eisenstein, O.; Loch, J.; Crabtree, R. H., *Inorg. Chem.*, **2001**, *40*, 5806.

(38) Herrmann, W. A., *Angew. Chem. Int. Ed.*, **2002**, *41*, 1291.

(39) (a) Weskamp, T.; Schattenmann, W. C.; Spiegler, M.; Herrmann, W. A. *Angew. Chem. Int. Ed.* **1998**, *37*, 2490. (b) Herrmann, W. A. *Angew. Chem. Int. Ed.* **1999**, *38*, 262.

(40) Albrecht, M.; Miecznikowski, J. R.; Samuel, A.; Faller, J. W.; Crabtree, R. H., *Organometallics,* **2002**, *21*, 3596.

(41) Perry, M. C.; Cui, X. H.; Powell, M. T.; Hou, D. R.; Reibenspies, J. H.; Burgess, K., *J. Am. Chem. Soc.,* **2003**, *125*, 113.

(42) Vazquez-Serrano, L. D.; Owens, B. T.; Buriak, J. M., *Chem. Commun.,* **2002**, 2518.

(43) Kuhl, S.; Schneider, R.; Fort, Y., *Organometallics,* **2003**, *22*, 4184.

(44) Edwards, M. G.; Jazzar, R. F. R.; Paine, B. M.; Shermer, D. J.; Whittlesey, M. K.; Williams, J. M. J.; Edney, D. D., *Chem. Commun.,* **2004**, 90.

(45) Dharmasena, U. L.; Foucault, H. M.; dos Santos, E. N.; Fogg, D. E.; Nolan, S. P., *Organometallics,* **2005**, *24*, 1056.

(46) Lee, H. M.; Smith, D. C., Jr.; He, Z.; Stevens, E. D.; Yi, C. S.; Nolan, S. P., *Organometallics,* **2001**, *20*, 794.

(47) Dinger, M. B.; Mol, J. C., *Eur. J. Inorg. Chem.,* **2003**, *15*, 2827.

(48) (a) Trnka, T. M.; Grubbs, R. H. *Acc. Chem. Res.* **2001**, *34*, 18. (b) Fürstner, A. *Angew. Chem. Int. Ed.* **2000**, *39*, 3012. (c) Fürstner, A.; Ackermann, L.; Gabor, B.; Goddard, R.; Lehmann, C. W.; Mynott, R.; Stelzer, F.; Thiel, O. R. *Chem. Eur. J.* **2001**, *7*, 3236. (d) Ivin, K. J. *J. Mol. Catal. A* **1998**, *133*, 1.

(49) Schrock, R. R.; Hoveyda, A. H., *Angew. Chem. Int. Ed.,* **2003**, 42, 4592.

(50) Hoveyda, A. H.; Schrock, R. R., *Chem. Eur. J.,* **2001**, 7, 945.

(51) Weskamp, T.; Schattenmann, W. C.; Spiegler, M.; Herrmann, W. A., *Angew. Chem. Int. Ed.*, **1998**, *37*, 2490.

(52) Weskamp, T.; Kohl, F. J.; Hieringer, W.; Gleich, D.; Herrmann, W. A., *Angew. Chem. Int. Ed.*, **1999**, *38*, 2416.

(53) Scholl, M.; Ding, S.; Lee, C. W.; Grubbs, R. H., *Org. Lett.*, **1999**, *1*, 953.

(54) Love, J. A.; Morgan, J. P.; Trnka, T. M.; Grubbs, R. H., *Angew. Chem. Int. Ed.*, **2002**, *41*, 4035.

(55) Sanford, M. S.; Love, J. A.; Grubbs, R. H., *Organometallics*, **2001**, *20*, 5314.

(56) Wakamatsu, H.; Blechert, S., *Angew. Chem. Int. Ed.*, **2002**, *41*, 2403.

(57) Wakamatsu, H.; Blechert, S., *Angew. Chem. Int. Ed.*, **2002**, *41*, 794.

(58) (a) Grela, K.; Harutyunyan, S.; Michrowska, A. *Angew. Chem. Int. Ed.* **2002**, *41*, 4038. (b) Michrowska, A.; Bujok, R.; Harutyunyan, S.; Sashuk, V.; Dolgonos, G.; Grela, K. *J. Am. Chem. Soc.* **2004**, *126*, 9318. (c) Zaja, M.; Connon, S. J.; Dunne, A. M.; Rivard, M.; Buschmann, N.; Jiricek, J.; Blechert, S. *Tetrahedron* **2003**, *59*, 6545.

(59) Schrock, R. R., *Acc. Chem. Res*, **1990**, *23*, 158.

(60) (a) O'Dell, R.; McConville, D. H.; Hofmeister, G. E.; Schrock, R. R. *J. Am. Chem. Soc.* **1994**, *116*, 3414. (b) Schrock, R. R.; Lee, J.-K.; O'Dell, R.; Oskam, J. H.; *Macromolecules*, **1995**, *28*, 5933. (c) Alexander, J. B.; La, D. S.; Cefalo, D. R.; Hoveyda, A. H.; Schrock, R. R. *J. Am. Chem. Soc.* **1998**, *120*, 4041. (d) La, D. S.; Alexander, J. B.; Cefalo, D. R.; Graf, D. D.; Hoveyda, A. H.; Schrock, R. R. *J. Am. Chem. Soc.* **1998**, *120*, 9720. (e) Zhu, S. S.; Cefalo, D. R.; La, D. S.; Jamieson, J. Y.; Davis, W. M.; Hoveyda, A. H.; Schrock, R. R. *J. Am. Chem. Soc.* **1999**, *121*, 8251. (f) La, D. S.; Ford, J. G.; Sattely, E. S.; Bonitatebus, P. J.; Schrock, R. R.; Hoveyda, A. H. *J. Am. Chem. Soc.* **1999**, *121*, 11 603.

(61) Schwab, P.; Grubbs, R. H.; Ziller, J. W., *J. Am. Chem. Soc.*, **1996**, *118*, 100.

(62) Amoroso, D.; Yap, G. P. A.; Fogg, D. E. *Organometallics* **2002**, *21*, 3335.

(63) Hong, S. H.; Day, M. W.; Grubbs, R. H., *J. Am. Chem. Soc.*, **2004**, *126*, 7414.

(64) Amoroso, D.; Snelgrove, J. L.; Conrad, J. C.; Drouin, S. D.; Yap, G. P. A.; Fogg, D. E. *Adv. Synth. Catal.* **2002**, *344*, 757.

(65) Sanford, M. S.; Henling, L. M.; Day, M. W.; Grubbs, R. H., *Angew. Chem. Int. Ed.*, **2000**, *39*, 3451.

(66) Campora, J.; Reyes, M. L.; Mereiter, K., *Organometallics,* **2002**, *21*, 1014.

(67) Poulton, J. T.; Hauger, B. E.; Kuhlman, R. L.; Caulton, K. G., *Inorg. Chem.*, **1994**, *33*, 3325.

(68) Snelgrove, J. L.; Conrad, J. C.; Eelman, M. D.; Moriarty, M. M.; Yap, G. P. A.; Fogg, D. E., *Organometallics,* **2005**, *24*, 103.

(69) Snelgrove, J. L.; Conrad, J. C.; Yap, G. P. A.; Fogg, D. E., *Inorg. Chim. Acta,* **2003**, *345*, 268.

(70) Conrad, J. C.; Amoroso, D.; Czechura, P.; Yap, G. P. A.; Fogg, D. E., *Organometallics,* **2003**, *22*, 3634.

(71) Drouin, S. D.; Foucault, H. M.; Yap, G. P. A.; Fogg, D. E., *Can. J. Chem.*, **2005**, *83*, 748.

(72) Monfette, S.; Fogg, D. E., *Organometallics,* **2006**, *25*, 1940.

CHAPTER 2

Experimental Procedures

2.1. Materials

Solvents. Reagent grade hexanes, dichloromethane, toluene, tetrahydrofuran and benzene were dried and degassed using a Glass Contour solvent purification system and stored over Linde 4Å molecular sieves. Methanol was refluxed over and distilled from CaH_2 under an atmosphere of N_2. Deuterated solvents ($CDCl_3$, C_6D_6 and toluene-d_8) were obtained from Cambridge Isotope Laboratories Ltd. $CDCl_3$ was refluxed over and distilled from CaH_2 under an atmosphere of N_2. C_6D_6 was dried over activated sieves (Linde 4Å) and degassed by consecutive freeze-pump-thaw cycles. Ampoules of toluene-d_8 were used as received. All deuterated solvents were stored under N_2.

Gases. Hydrogen (Praxair, UHP Grade) and nitrogen (Praxair, Research Grade) were used as received for all reactions.

Substrates. Cyclododecene, allylbenzene and cyclooctene were purchased from Aldrich Chemical Co., passed through a column of neutral alumina and distilled under vacuum. All substrates were stored under an atmosphere of N_2.

Other Materials. Hydrated $RuCl_3$ (38-43% Ru) and triphenylphosphine were purchased from Strem Chemical Co. and used as received. Tetralin, pyrrole-2-carboxaldehyde, 2, 6-

diisopropylaniline, *n*-butyllithium (*n*-BuLi, 1.6 M in hexanes), 1, 4-dibromobutane, dicyclohexylphosphine, tricyclohexylphosphine, *p*-toluenesulfonhydrazide and benzaldehyde were obtained from Aldrich Chemical Co. Tetralin, *n*-butyllithium, dicyclohexylphosphine and tricyclohexylphosphine were stored in a drybox under an atmosphere of N_2.

2.2. Instrumentation

Routine solution nuclear magnetic resonance (NMR) spectra were recorded on a Bruker Avance-300 (300 MHz for ^1H, 121 MHz for ^{31}P and 75 MHz for ^{13}C) or a Bruker Avance-500 (500 MHz for ^1H, 202 MHz for ^{31}P and 125 MHz for ^{13}C) FT-NMR spectrometer. Variable-temperature (VT) NMR, as well as all solution 2D NMR experiments, including ^1H correlation (COSY), ^1H-^{13}C heteronuclear multiple quantum coherence (HMQC), ^1H-^{13}C heteronuclear multiple bond coherence (HMBC) and ^{31}P exchange spectroscopy (EXSY) spectra were recorded on a Bruker Avance-500 FT-NMR spectrometer. For ^1H and ^{13}C spectra, signals are reported in parts per million (ppm) relative to TMS (0 ppm) while the residual proton and carbon signals of the deuterated solvent were used as secondary internal chemical shift references. ^{31}P NMR spectra were reported relative to externally referenced 85 % H_3PO_4 at 0 ppm. Pulsed field gradient spin echo (PGSE) diffusion NMR measurements were recorded on a Bruker Avance-500 FT-NMR spectrometer. Solid-state ^{31}P NMR analysis of powdered samples were performed at 4.7 T (81.0 MHz) and 11.75 T (202.47 MHz) using Bruker ASX and Avance consoles, respectively. IR spectra were measured on a Bomem MB100 IR spectrometer. Inert atmosphere MALDI-TOF analysis was performed using a Bruker OmniFlex MALDI-TOF spectrometer equipped with a nitrogen laser (337 nm) and interfaced to an MBraun glovebox. Data were collected in positive reflectron mode, with the accelerating voltage held at 20 kV. Pyrene matrix

and analyte solutions were prepared in CH_2Cl_2 at concentrations of 20 and 1 mg/L, respectively. Samples were mixed in a matrix:analyte ratio of 20:1. Microanalysis was carried out by Guelph Chemical Laboratories Ltd., Guelph, Ontario.

2.3. Laboratory Techniques

Unless otherwise stated, all reactions were carried out at room temperature (RT, ≈ 22 °C) under an inert atmosphere of nitrogen using standard Schlenk or drybox techniques.

2.4. Literature Preparations

The following compounds were kindly provided by Ureshini Dharmasena (Fogg Group, University of Ottawa): $RuHCl(CO)(PCy_3)_2$ (**1**),[1] $RuHCl(CO)(IMes)(PCy_3)$ (**2**) (IMes = 1, 3-bis(2,4,6-trimethylphenyl)imidazolin-2-ylidene),[2] $RuHCl(CO)(IMes)(PPh_3)$ (**3**)[3] and $RuHCl(CO)(H_2IMes)(PPh_3)$ (**4**).[3] The following compounds were prepared according to literature precedent: $RuCl_2(PPh_3)_3$ (**5**),[4] *N'*-benzylidene-4-methylbenzenesulfonohydrazide,[5] phenyldiazomethane,[6] $RuCl_2(CHPh)(PCy_3)_2$,[7] $RuCl(\kappa^2\text{-}C, N\text{-}ArN{=}CHC_4H_3N)(PCy_3)(CHPh)$ (**9a**) (Ar =2,6-*i*-$Pr_2C_6H_3$),[8] 1,4-bis(dicyclohexylphosphino)butane (dcypb),[9] and $Ru_2Cl_4(dcypb)_2(N_2)$ (**10**).[9]

2.5. General Procedure for Catalytic Hydrogenation Experiments

A representative procedure is given for the hydrogenation of cyclododecene. In a glovebox, a Parr autoclave was charged with cyclododecene (0.333g, 2.00 mmol), toluene (15 mL) and $RuHCl(CO)(H_2IMes)(PPh_3)$ (**4**) (0.73 mg, 1.00 μmol). The sealed autoclave was removed from the drybox, purged with H_2 (with stirring), pressurized to 140 psi and heated to 80

°C. The sample reached thermal equilibrium in seven minutes, at which point the sample designated t = 0 h was removed. Subsequent samples were removed at 0.5 h, 1 h and 2 h. Product yields were determined by gas chromatographic analysis and integrated against tetralin as an internal standard. An average of two trials is reported (±3%).

2.6. Computational Details

All calculations were performed using the Jaguar 6.0 software package.[10] Energies and geometry optimizations of the stationary points (reactants, products, intermediates and transition states) reflect the use of quantum chemical[11] density functional theory and implementation of Becke's three parameter hybrid gradient-corrected exchange functional[12] and the gradient-corrected functional of Lee, Yang and Parr,[13] abbreviated as B3LYP. In conjunction with the above, the LACVP** basis set was used.[14] The core electrons of ruthenium are represented with an effective core potential and the outermost valence orbitals are accounted for. Atoms not including ruthenium (i.e. H, C, O, P and Cl) are represented using the 6-31G** basis set developed by Pople and co-workers.

Frequency calculations were performed on all stationary points to confirm that minimum energy structures had no imaginary frequencies and that transition states had only one imaginary frequency. All of the energies include unscaled zero-point energy corrections. It is reasonable to assume that the located transition states correspond to the reaction pathway of interest based on a comparison of geometries, relative energies and bond orders of the ensemble of stationary points.

A smaller model system was used for the catalysts where tricyclohexylphosphine, in the case of **1**, and triphenylphosphine, in the case of $RuHCl(PPh_3)_3$, are both represented by the PH_3 ligand. This is a typical approach used in quantum chemical calculations to reduce

computational time. The effect of these substitutions is not expected to have any bearing of the qualitative nature of these calculations.

2.7. Pyrrole Ligand Precursors and Ru-Pyrrole Complex

2.7.1. 2-[(2, 6-Diisopropylphenyl)imino]pyrrole (HNN') (6)

In a modification of a literature procedure,[15, 16] a solution of 2,6-diisopropylaniline (5 mL, 26 mmol) and pyrrole-2-carboxaldehyde (2.5 g, 26 mmol) in methanol:benzene (1:4, total volume = 25mL) was refluxed using a Dean-Stark apparatus for 4 days. The reaction mixture was reduced to half of its original volume, yielding a yellow oil. Upon treatment with methanol, a white precipitate was observed, and the resulting suspension was cooled to 0 °C for 4 h. This was then filtered cold, washed with cold methanol (5 × 10 mL) and dried in vacuo. A second crop was obtained by concentration of the filtrate and precipitation with cold methanol. Combined yield: 4.9 g (73%). NMR data agree with those values reported.[16] ^{1}H NMR (C_6D_6, δ): 10.46 (br s, 1 H, NH), 7.84 (br s, 1 H, N=C*H*), 7.18 (br s, 3 H, Ar), 6.45 (br m, 1 H, pyr H_5), 6.05 (br m, 2 H, pyr H_4 and H_3), 3.24 (sept, $^3J_{HH}$ = 6.8 Hz, 2 H, 2 × C*H*Me_2), 1.12 (d, $^3J_{HH}$ = 6.8 Hz, 12 H, 2 × CH_3).

2.7.2. Lithium 2-[(2, 6-Diisopropylphenyl)imino]pyrrolide (LiNN') (7)

In a modification of a literature method,[15] LiNN' was obtained free of a solvating molecule of diethyl ether[8] by addition of *n*-BuLi (1.6 M solution in hexanes, 5.5 mL, 8.85 mmol) in 2 mL of hexanes to a solution of **6** (1.84 g, 7.25 mmol) in 40 mL of hexanes at –80 °C. The reaction mixture was stirred at –80 °C for 2 h, then stripped of solvent to yield an off-white solid.

This solid was then re-dissolved in the minimal amount of hexanes (10 mL), cooled to –35 °C and then filtered. Yield: 1.4 g (74%). The product was stored at -35°C under N_2. NMR data agree with those reported,[15] excluding the solvating molecule of diethyl ether. ^{1}H NMR (C_6D_6, δ): 8.02 (br s, 1 H, N=C*H*), 7.40-7.15 (br m, 4 H + pyr H_5), 6.89 (br m, 1 H, pyr H_4), 6.42 (br m, 1 H, pyr H_3), 3.42 (sept, $^3J_{HH}$ = 6.8 Hz, 2 H, 2 × C*H*Me_2), 1.12 (d, $^3J_{HH}$ = 6.8 Hz, 12 H, 2 × CH_3).

2.7.3. [RuCl(κ^2-*N,N'*-ArN=CHC$_4$H$_3$N)(PPh$_3$)$_2$]$_2$ (Ar = 2,6-^{i}Pr$_2$C$_6$H$_3$) (8)

Addition of solid LiNN' (**7**) (626 mg, 2.40 mmol) to a dark brown solution of **5** (1.27 g, 1.30 mmol) in CH_2Cl_2 (30 mL) resulted in a colour change to black. Stirring of the black solution was continued for 12 h, after which the solvent was removed in vacuo. The resulting black, oily solid was dissolved in 10 mL hexanes and chilled to –30 °C to afford a dark purple precipitate. This was filtered cold, washed with cold hexanes (3 × 10 mL) and dried in vacuo. Yield: 1.7 g (72%). Low yields are incurred by the high solubility of this compound in all hydrocarbon solvents, including pentane. ^{31}P{^{1}H} NMR (C_6D_6, δ): 58.5 (s, PPh_3). ^{1}H NMR (C_6D_6, δ): 7.90 (t, $^4J_{HP}$ = 2.1 Hz, 1 H, N=C*H*), 7.29-6.85 (m, 33 H, Ph, Ar), 7.15 (br s, 1 H pyr H_5), 6.34 (m, 1 H, pyr H_4), 6.18 (br s, 1 H, pyr H_3), 2.48 (sept, $^3J_{HH}$ = 7 Hz, 2 H, 2 × C*H*Me_2), 0.90 (d, $^3J_{HH}$ = 7 Hz, 6 H, 2 × CH_3), 0.83 (d, $^3J_{HH}$ = 7 Hz, 6 H, 2 × CH_3). ^{13}C{^{1}H} NMR (C_6D_6, δ): 164.2 (s, N=*C*H), 147.5 (s, pyr C_2), 144.1 (s, Ar C_1), 143.7 (s, pyr C_3), 143.0 (s, Ar C_2, C_6), 135.0-135.5 (multiple s, Ph), 126.8 (s, Ar C_4), 123.4 (s Ar C_3, C_5), 121.3 (s, pyr C_5), 114.5 (s, pyr C_4), 29.4 (s, 2 × *C*HMe_2), 26.5 (s, CH_3), 22.7 (s, CH_3). Anal. Calc'd. For $C_{106}H_{102}Cl_2N_4P_4Ru_2$: C, 69.91; H, 5.62; N, 3.06%. Found: C, 69.12; H, 5.67; N, 2.79%. MALDI-TOF MS, *m/z*: Calc'd for [Ru_2Cl_2(NN')(PPh_3)$_4$]$^{+\bullet}$, 1828.5; Found, 1044.2 (corresponds to [M-3PPh_3 + 2H]$^+$). Calc'd for [RuCl(NN')(PPh_3)]$^{+\bullet}$: 652.1; Found, 652.3.

2.8. Solid-State NMR Spectroscopy

These experiments were conducted by Dr. David Bryce (University of Ottawa). ^{31}P NMR spectra of powdered samples were recorded at 4.7 T (81.0 MHz for ^{31}P) and 11.75 T (202.47 MHz for ^{31}P) using Bruker ASX and Avance consoles, respectively. For experiments at 4.7 T, custom Teflon inserts were packed in a glovebox, under nitrogen, and placed inside zirconia rotors (7 mm o.d.) for use in a Bruker double-resonance magic-angle spinning (MAS) probe. For experiments at 11.75 T, zirconia rotors of 4 mm o.d. were used in a Bruker triple-resonance MAS probe. ^{31}P chemical shifts were referenced externally to 85 % H_3PO_4 at 0 ppm using solid ammonium dihydrogen phosphate as a secondary reference δ_p = + 0.81 ppm.[17] ^{31}P spectra were obtained using cross-polarization (CP) from ^{1}H, and free induction decays (FIDs) were acquired with high-power proton decoupling. Typical $\pi/2$ pulses were 4.0-4.5 μs at 4.7 T and 3.0-3.3 μs at 11.75 T. Typical CP contact times were 2-3 ms and typical recycle delays were 10 s. Regular CP experiments and standard MAS probes were used for recording spectra of stationary samples. 1D data were processed (exponential multiplication, zero-filling) using Bruker's XWINNMR software. Spectral simulations were performed using WSOLIDS1.[18]

Two-dimensional ^{31}P-^{31}P COSY, spin-echo correlation spectroscopy (SECSY) and *J*-resolved spectroscopy experiments[19, 20] were performed at 4.7 T while 2D *J*-resolved spectra were also obtained at 11.75 T. The pulse sequences for the these experiments are summarized CP-t_1-$\pi/2(^{31}P)$-ACQ(t_2) (COSY); CP-$t_1/2$-$\pi/2(^{31}P)$-$t_1/2$-ACQ (SECSY); CP-$t_1/2$-$\pi(^{31}P)$-$t_1/2$-ACQ (*J*-resolved). The phase cycling used is given by Wu and Wasylishen.[21] All 2D experiments were recorded in a rotor-synchronized fashion. As an example, for *J*-resolved experiments at 11.75 T with an MAS rate of 5 kHz, the t_1 increment was 200 μs. Typically 128 or 256 t_1 increments were used. An MAS rate of 5.3 kHz was used for 2D experiments recorded at 4.7 T.

Data were apodized by a cosine function in the directly detected dimension and by a squared cosine function in the indirect dimension. The resulting data were zero-filled at least once in each dimension followed by 2D Fourier transformation and displayed in magnitude mode. All 2D datasets were processed and analyzed using nmrPipe.[22]

2.9. Pulsed Field Gradient Spin Echo (PGSE) Diffusion NMR

^{1}H PGSE NMR measurements were performed in $CDCl_3$ (15 mM, 22 °C) on a Bruker Avance-500 spectrometer according to the standard (Stejskal-Tanner) pulse sequence.[23, 24] Transverse magnetization was induced by an initial $\pi/2$ pulse. Application of the first of two pulsed linear field gradients for a fixed period of time (δ = 4 ms) strongly dephases the magnetization. Following subsequent application of a π pulse, a second pulsed linear field gradient exactly equal to and at a fixed time interval from the first (Δ = 10 ms) is applied reversing the respective phases and generating an echo. Gradient strength (G) is increased in subsequent experiments in increments of 10% from 0% to 100% (or from 8.51×10^{-4} Tm^{-1} to 0.524 Tm^{-1}).

Values for the translational diffusion constant (D) were calculated from experimentally-derived integral intensities I (I_0 = intensity at zero gradient strength) according to equation 4.1, using a value of 2.675×10^8 $T^{-1}m^{-1}$ for the gyromagnetic ratio (γ) of the ^{1}H nucleus. All spectra were acquired using 16 scans and 64K points, with a spectral width of 7440 Hz, and processed with a line broadening of 1 Hz. Gradient calibration carried out on HOD in D_2O gave a diffusion constant of 1.98×10^{-9} m^2s^{-1} (correlation > 0.99) which is in acceptable agreement to the literature precedent of 2.0×10^{-9} m^2s^{-1}.[24-26]

2.10. References

(1) Yi, C. S.; Lee, D. W., *Organometallics,* **1999**, *18*, 5152.

(2) Lee, H. M.; Smith, D. C., Jr.; He, Z.; Stevens, E. D.; Yi, C. S.; Nolan, S. P., *Organometallics,* **2001**, *20*, 794.

(3) Dharmasena, U. L.; Foucault, H. M.; dos Santos, E. N.; Fogg, D. E.; Nolan, S. P., *Organometallics,* **2005**, *24*, 1056.

(4) Hallman, P. S.; Stephenson, T. A.; Wilkinson, G., *Inorg. Synth.,* **1970**, *12*, 237.

(5) Creary, X., *Organic Syntheses,* **1990,** VII, 438.

(6) Yates, P.; Shapiro, B. L., *J. Org. Chem.,* **1958**, *23*, 759.

(7) Schwab, P.; Grubbs, R. H.; Ziller, J. W., *J. Am. Chem. Soc.,* **1996**, *118*, 100.

(8) Drouin, S. D.; Foucault, H. M.; Yap, G. P. A.; Fogg, D. E., *Can. J. Chem.,* **2005**, *83*, 748.

(9) Amoroso, D.; Yap, G. P. A.; Fogg, D. E., *Can. J. Chem.,* **2001**, *79*, 958.

(10) *Jaguar 6.0*, Schrodinger, LLC: Portland, Oregon, **2004**.

(11) Ziegler, T.; Autschbach, J., *Chem. Rev.,* **2005**, *105*, 2695.

(12) Becke, A. D., *J. Chem. Phys.,* **1993**, *98*, 5648.

(13) Lee, C.; Yang, W.; Parr, R. G., *Phys. Rev. B.: Condens. Matter,* **1988**, *37*, 785.

(14) Hay, P. J.; Wadt, W. R., *J. Chem. Phys.,* **1985**, *82*, 299.

(15) Dawson, D. M.; Walker, D. A.; Thornton-Pett, M.; Bochmann, M., *J. Chem. Soc., Dalton Trans.*, **2000**, 459.

(16) Matsuo, Y.; Mashima, K.; Tani, K., *Chem. Lett.*, **2000**, 1114.

(17) Bryce, D. L.; Bernard, G. M.; Gee, M.; Lumsden, M. D.; Eichele, K.; Wasylishen, R. E., *Can. J. Anal. Sci. Spectros.*, **2001**, *46*, 46.

(18) Eichele, K., Wasylishen, R. E. *WSOLIDS NMR Simulation Package*, 1.17.30; Dalhousie University: Halifax, **2001**.

(19) Wu, G.; Wasylishen, R. E.; Curtis, R. D., *Can. J. Chem.*, **1992**, *70*, 863.

(20) Wu, G.; Wasylishen, R. E., *Inorg. Chem.*, **1992**, *31*, 145.

(21) Wu, G.; Wasylishen, R. E., *Organometallics*, **1992**, *11*, 3242.

(22) Delaglio, F.; Grzesiek, S.; Vuister, G. W.; Zhu, G.; Pfeifer, J.; Bax, A., *J. Biomol. NMR*, **1995**, *6*, 277.

(23) Stejskal, E. O.; Tanner, J. E., *J. Chem. Phys.*, **1965**, *42*, 288.

(24) Stilbs, P., *Prog. Nucl. Magn. Reson. Spectrosc.*, **1987**, *19*, 1.

(25) Tyrell, H. J. V.; Harris, K. R., *Diffusion in Liquids: A Theoretical and Experimental Study*. 1984; p 448.

(26) Berger, S.; Braun, S., *200 and More NMR Experiments: A Practical Course*. Wiley-VCH: Weinheim, Germany, 2004; p 838.

CHAPTER 3

Quantum Chemical Study and Catalytic Activity Investigation of Ruthenium Hydridocarbonyl Complexes

3.1. Introduction

Addition of H_2 across a double bond requires use of a metal catalyst to overcome the symmetry restrictions associated with a concerted *cis* addition.[1] Heterogeneous systems, including Raney nickel, palladium on carbon (Pd/C), and platinum on alumina,[2,3] can effect this transformation easily for many functional groups, and under a variety of conditions. However, reduction of unsaturated bonds is largely indiscriminate, partial disproportionation can occur and catalysts loadings are high (in some cases stoichiometric). Hydrogenation by soluble transition metal complexes offers tremendous potential for control over catalyst activity, enabling regio-, chemo-, and stereo-selectivity, as well as overall system productivity. Homogeneous transition metal catalysts are able to stabilize ligands of varying electronic character, which in turn give access to a range of oxidation states and coordination numbers.

While many transition metal complexes effect hydrogenation of unsaturated bonds,[2] late metals from groups 8 to 10 are generally the most active. The majority of such catalysts contain rhodium, iridium or ruthenium. Wilkinson's catalyst, $RhCl(PPh_3)_3$, can be purchased commercially or synthesized from reaction of $RhCl_3 \cdot 3H_2O$ with PPh_3 in ethanol.[4] It is routinely used to hydrogenate olefins of minimal substitution under ambient conditions.[5] Disadvantages of its use include a tendency to decarbonylate aldehydes and allylic alcohols, which can deactivate the catalyst, and a low activity for the reduction of tri- and tetrasubstituted olefins.[6] The Crabtree catalyst, $[Ir(COD)(PCy_3)(py)]^+$, is remarkably effective for the hydrogenation of highly-

substituted double bonds[7] but susceptible to decomposition into a catalytically-inactive tri-iridium complex.[8] Ruthenium catalysts have attracted attention for use in hydrogenation, owing to their relatively low cost, an ability to stabilize ligands by back-bonding, a tendency to undergo intra and intermolecular metallation and facile formation of polyhydride compounds.[5] Hydrogenation of simple olefins is typically more effective with Ir and Rh catalysts, rather than Ru.[5] However, the relatively mild reaction conditions typically associated with ruthenium-mediated hydrogenations makes this class of catalysts particularly attractive for the chemoselective hydrogenation of polyolefins.[9] Other substrates that can be reduced by ruthenium catalysts include: alkenes,[10-13] alkynes,[14] carbonyls,[15-17] imines, [18,19] and aromatics.[20-22]

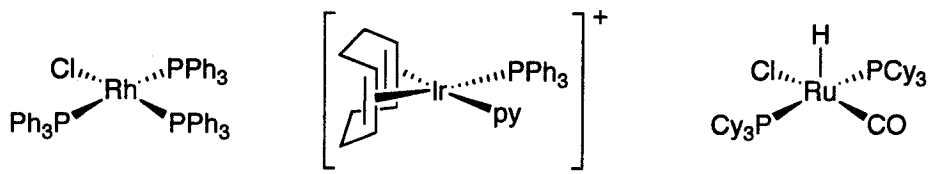

A B C

Figure 3.1 Representative hydrogenation catalysts: Wilkinson's catalyst (**A**), Crabtree's catalyst (**B**) and the Yi catalyst (**C**).

$RuHCl(PPh_3)_3$ enables hydrogenation of terminal alkenes under ambient conditions.[5] For reduction of more challenging substrates, increased catalyst activity is required. This can be achieved by use of analogues containing more basic donor ligands. In early work examining the effect of phosphine basicity on the rate of olefin reduction, the reactivity of catalyst $RuCl_2[P(p\text{-}XC_6H_4)_3]_3$ was shown to follow the trend X = H < CH_3 < OCH_3.[23] Substitution of PPh_3 in $RuHCl(CO)(PPh_3)$ by PCy_3, generating $RuHCl(CO)(PCy_3)_2$, substantially increases catalytic activity,[24] due to both a decrease in coordination number and an increase in ligand basicity.[12] Interestingly, however, introduction of an *N*-heterocyclic carbene ligand in the latter complex

results in a *decrease* in catalytic activity. For example, the rate of hydrogenation of 1-hexene by $RuHCl(CO)(IMes)(PCy_3)$ compares to that of $RuHCl(CO)(PCy_3)_2$ only at temperatures above 100 °C (IMes = bis(1,3-mesityl-imidazol-2-ylidene); (Figure 3.2).[24-26] The increased σ-donating ability and two-dimensional steric demand of the *N*-heterocyclic carbene should reasonably have promoted olefin binding and activation by $RuHCl(CO)(IMes)(PCy_3)$ (**2**).[27] Our group speculated that the reduced activity of **2** results from the low lability of a PCy_3 ligand *trans* to a *N*-heterocyclic carbene. Precedent for such behaviour was found in metathesis by $RuCl_2L(PCy_3)(CHPh)$, for L = IMes versus PCy_3.[28] Substitution of the PCy_3 ligand in **2** by a more labile ancillary ligand, such as PPh_3 or pyridine, should thus increase hydrogenation activity.

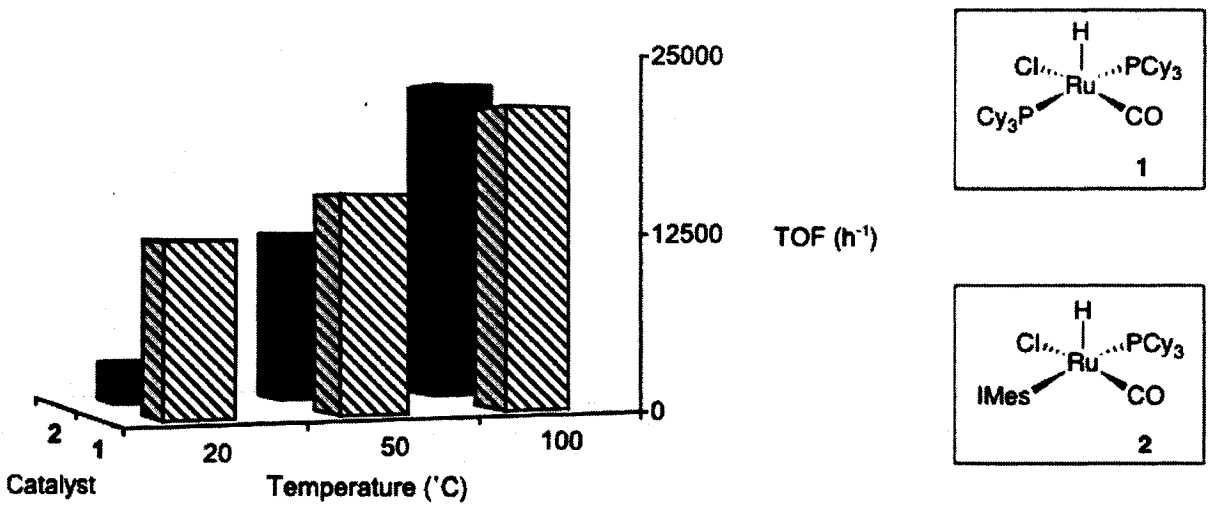

Figure 3.2 Comparative reactivities of $RuHCl(CO)(PCy_3)_2$ (**1**) and $RuHCl(CO)(PCy_3)(IMes)$ (**2**) for the hydrogenation of 1-hexene.[24-26]

The rate of olefin hydrogenation by hydrido carbonyl complexes of Ir and Rh is impaired by incorporation of a π-acidic ligand, such as CO. This effect has been linked to the inhibition of H_2 oxidative addition to the metal centre.[2,4,29] Introduction of a CO ligand into analogous complexes of ruthenium, however, has mixed effects on the rate of olefin reduction. $RuHCl(CO)(PPh_3)_3$ has reduced activity, relative to $RuHCl(PPh_3)_3$, for the hydrogenation of simple olefins.[5,30] This is due to the kinetic stability of the former catalyst afforded by its coordinative saturation, preventing generation of active species $RuHCl(CO)(PPh_3)$. Ruthenium hydridocarbonyl catalysts containing alkylphosphines, however, are coordinatively unsaturated and have activities superior to analogous complexes without a CO ligand. Samantha Drouin of this research group has documented this effect by comparing the rate of allylbenzene reduction mediated by $RuHCl(CO)(PCy_3)_2$ and $RuHCl(H_2)(PCy_3)_2$.[31] Conversions to propylbenzene were 80 % and 31 %, respectively, for the two catalysts. In addition, the turnover frequency for

$RuHCl(CO)(PCy_3)_2$ was an order of magnitude higher than that for $RuHCl(H_2)(PCy_3)_2$. As an explanation for the rate enhancement afforded by $RuHCl(CO)(PCy_3)_2$ and analogues, it was proposed that CO may destabilize the transient Ru(IV) intermediate resulting from activation of H_2, thus favouring elimination of the saturated product (Scheme 3.1). Evidence for this explanation is circumstantial, based solely on the recent observation of Ru(IV) complexes in situ.[32]

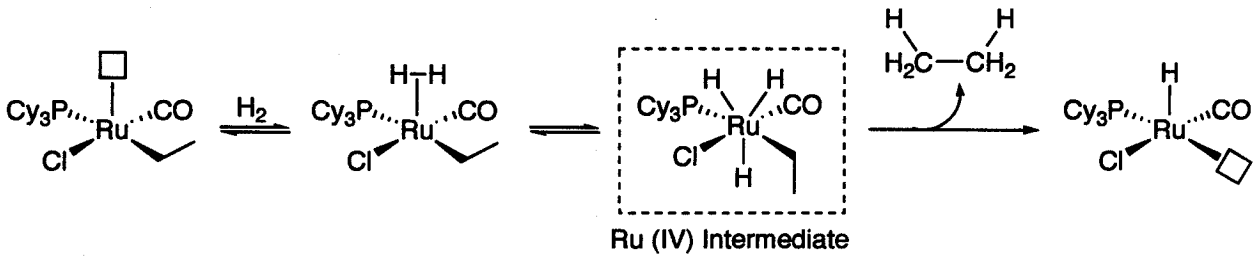

Scheme 3.1 Proposed route for generation of a Ru (IV) intermediate.

Additional data to support a possible activating effect accompanying incorporation of a CO ligand into ruthenium systems, where this ligand is pre-installed and the resulting catalyst has been isolated, are scarce. Indirect evidence from tandem metathesis-hydrogenation experiments reaffirms the enhanced activity of hydrido carbonyl ruthenium catalysts. The hydrogenation step, starting from a ruthenium-alkylidene, is facilitated in the presence of methanol and triethylamine.[33] This enhancement is probably due to the decarbonylation of methanol by ruthenium, generating a hydrido carbonyl catalyst *in situ*.[10,34]

3.2. Catalytic Activities of Complexes 1-4

The synthesis and characterization of **3** and **4** were carried out by Ureshini Dharmasena of the Fogg group at the University of Ottawa (Figure 3.3).[11] Benchmark catalysts were chosen based on high activity (**1**) and on the presence of a *N*-heterocyclic carbene (**2**). As the high hydrogenation activity of **1** is well established for terminal and activated alkenes,[25,26] the chosen targets for comparative catalytic studies were internal, unactivated olefins, a class of substrates for which few catalysts are effective.[35] Initial efforts focused on low catalyst loadings (0.05 mol% Ru), a condition with which the highly-active Ir systems are generally incompatible as they tend to deactivate at concentrations < 1 mol%.[36]

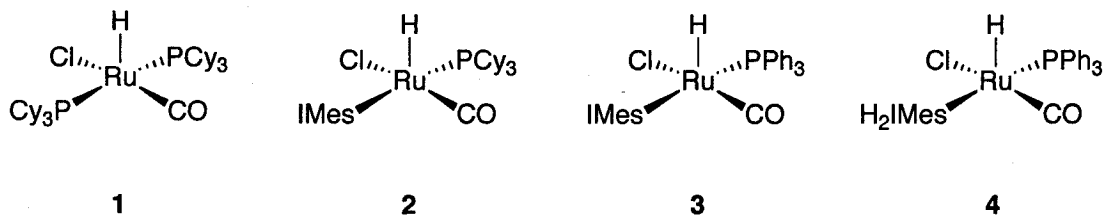

1 **2** **3** **4**

Figure 3.3 Benchmark (**1** and **2**) and novel, highly-active (**3** and **4**) Ru-hydrogenation catalysts.

The first target substrate, cyclooctene (COE) was chosen as a test system for the potential hydrogenation of larger macrocycles. This important class of compounds is directly relevant to the synthesis of saturated odiferous or organoleptic compounds[37] by tandem RCM-hydrogenation.[38,39] Reduction of COE suggested the trend **4** ≈ **2** > **1** (Table 3.1), with the *N*-heterocyclic carbene catalysts effecting complete conversion at 50 psi H_2 and 80 °C (GC analysis). Closer examination showed that the integrated intensity for the cyclooctane signal (where reduction had been catalyzed by *N*-heterocyclic carbene systems) is low relative to that of the internal standard when catalysts **2** and **3** were used. Approximately 20% polymer was

obtained by removal of volatile species (solvent, cyclooctane) under vacuum. Subsequent analysis by IR spectroscopy revealed that the resulting polymer was completely hydrogenated by **4** (polymer is too insoluble for NMR and GPC analysis), a process which normally occurs with difficulty.[40,41] A competition between undesirable ring-opening metathesis polymerization (ROMP) and hydrogenation activity may be deduced (Scheme 3.2). This suggests that the *N*-heterocyclic carbene catalysts may be best applied to systems where ring strain is low or negligible, and the susceptibility of the substrates to ROMP is thus minimal.

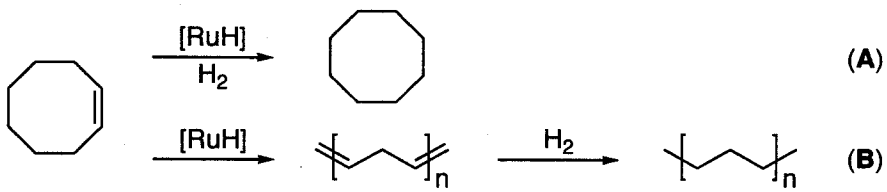

Scheme 3.2 The relationship between hydrogenation (**A**) and ROMP-hydrogenation (**B**).

The hydrogenation of cyclododecene (CDE, Scheme 3.3), a 12-membered macrocycle of comparatively low ring-strain (relative to COE[42]), was performed next. Hydrogenation of macrocyclic compounds is typically difficult due to their steric bulk and, more importantly, the mixture of *cis* and sterically-hindered *trans* isomers present in mixtures of these larger, cyclic internal olefins. This is best illustrated in the product distributions for hydrogenation of CDE (Figure 3.4): the quantity of *trans* CDE present after 1 h is virtually unchanged for catalysts **1** and **2**, while hydrogenation of both isomers by **3** and **4** occurs with considerably less difficulty; 10 times faster than **2** and 3-4 times faster than **1**.

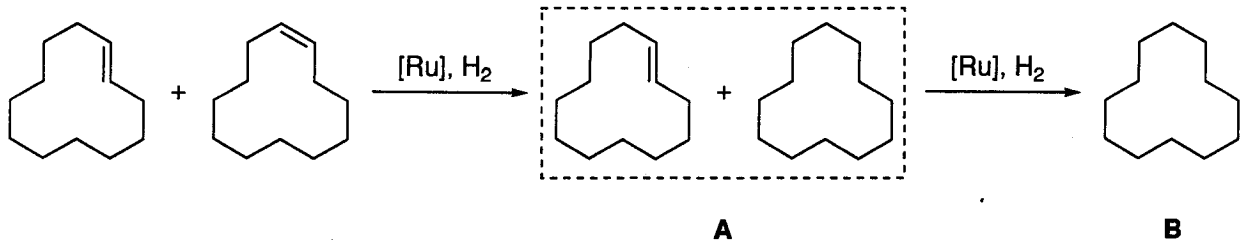

Scheme 3.3 Schematic representation of cyclododecene hydrogenation: *cis*-cyclododecene is hydrogenated first (**A**), followed by hydrogenation of the *trans* isomer (**B**).

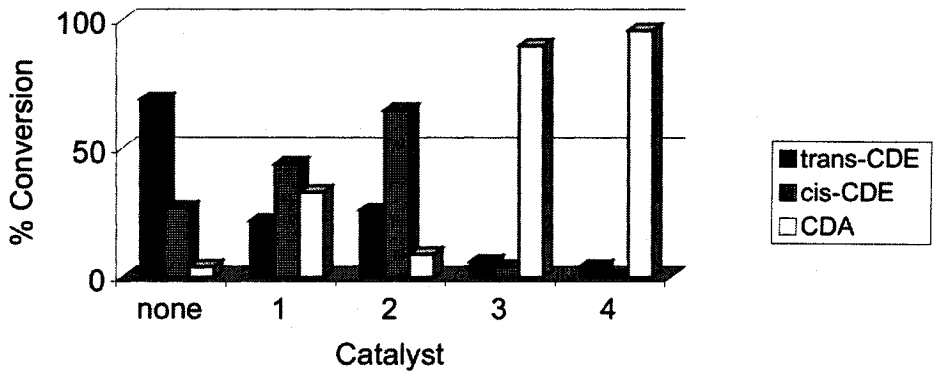

Figure 3.4 Product distributions at 1 h for reduction of cyclododecene (for reaction conditions see Table 3.1).

As seen in Table 3.1, there are two trends for hydrogenation activity. For COE, catalyst activity is **3** ≈ **2** > **1**, but the enhanced activity of the *N*-heterocyclic carbene systems is an artifact of their increased ability to polymerize the substrate. For hydrogenation of CDE, where polymerization is not as likely, catalyst reactivities follow the trend **4** > **3** >> **1** >>> **2**. For catalysts **3** and **4**, activity is significantly enhanced relative to the parent PCy_3 complex. This suggests that *N*-heterocyclic carbenes activate catalysts for hydrogenation provided that a highly labile ancillary ligand, such as PPh_3, exists *trans* to it.

Table 3.1 Hydrogenation of selected internal olefins[a].

Catalyst	Substrate	TOF[b]	Time (min)	Conversion (%)[c]
1	COE	138	10	69[d]
2		164[e]	10	100
3		164[e]	10	100
1	CDE	840	60	33
2		280	60	8
3		2840	60	90[d]
4		3880	60	96[d]

[a]Conditions: 0.05 mol % Ru, 2.0 mmol substrate, 50 psi of H_2 (COE); 140 psi of H_2 (CDE), 80 °C; toluene. [b] Turnover frequency calculated at 10 min (COE) and 30 min (CDE). Values are in units of min^{-1} for COE and h^{-1} for CDE. [c] Conversions determined by GC; ± 3% in replicate runs. The thermal equilibrium period was 7 min for 80 °C (t_0). [d] The conversion was 100% within 30 min (COE) and 2 h (CDE). [e] TOF corrected for ROMP contribution (18%).

Olefin isomerization is known to be mediated by metal hydrides, and can complicate hydrogenation reactions.[43] Isomerization can be problematic for any highly-active system, including **3** and **4**, if it occurs on the timescale of hydrogenation. The reduction of allylbenzene was pursued as a sensitive probe for olefin isomerization. Both **1** and **2** isomerize 9% of the allylbenzene but **1** effectively reduces 72% of this substrate, versus 51% for **2** (Table 3.2). Neither **1** nor **2** were able to reduce the *trans* olefin, even with an increase in pressure to 140 psi of H_2. Both **3** and **4** effect greater isomerization and enable hydrogenation of the *trans* olefin even at 50 psi H_2. The high isomerization activity of **4**, under the forcing conditions necessary to reduce the *trans* olefin, makes it less attractive as a potential hydrogenation catalyst for isomerizable double bonds.

Table 3.2 Reduction versus isomerization for allylbenzene.[a]

Catalyst	$p(H_2)$ (psi)	Propylbenzene (%)	PhCHCHMe (%)		TOF (h^{-1})[b]
			cis	*trans*	
1	50	72	0	9	2880 (360)
	140	86	0	9	3440 (360)
2	50	51	1	6	2040 (280)
	140	94	0	6	3760 (240)
3	50	60	0	40	2400 (1600)
	140	89[c]	0	11	3560 (440)
4	140	49	10	37	1960 (1880)

[a] Conditions: 0.05 mol % of Ru, 2.0 mmol of allylbenzene in toluene, 80 °C; 30 min reaction time following 't_0'. Conversions were determined by GC; ± 3% in replicate runs. [b] Turnover frequencies for hydrogenation; TOF values for isomerization are given in parentheses. [c] 100% at 2 h.

3.3. Computational Investigation of Increased Activity in Ruthenium Hydridocarbonyl Complexes

The basis for the following computations is that olefin reduction mediated by ruthenium (II) hydrido phosphine systems proceeds via a dissociative mechanism (Scheme 3.4).[5,30] This has been established via kinetics measurements and the resulting rate law[44] for Ru-catalyzed hydrogenation is outlined in Equation 3.1.

$$RuHCl(PPh_3)_3 \overset{K_1}{\rightleftharpoons} RuHCl(PPh_3)_2 + PPh_3$$

$$RuHCl(PPh_3)_2 + alkene \overset{K_2}{\rightleftharpoons} RuCl(PPh_3)_2(alkyl)$$

$$RuCl(PPh_3)_2(alkyl) + H_2 \xrightarrow{k} RuHCl(PPh_3)_2 + alkane$$

Scheme 3.4 Simplified kinetic pathway showing dissociative mechanism for Ru-hydrogenation.

$$\frac{-d[H_2]}{dt} = \frac{kK_2[Ru]_{Total}[olefin][H_2]}{1 + K_2[olefin] + [PPh_3]/K_1} \qquad (3.1)$$

Inspection of Equation 3.1 shows that the rate of ruthenium-catalyzed hydrogenation should be first order in H_2, between zero and first-order in olefin and inversely dependent on phosphine concentration. Aside from this, relatively little is known about the relationship between intermediate steps in the catalytic cycle. Quantum chemical investigations have helped to further the understanding of isolated steps, including: the orientation of hydrides in a metal-hydride complex,[45] olefin insertion into Ru-H bonds[46] and Ru-H and Ru-H_2 interactions.[47] The complete reaction pathway for the ruthenium-catalyzed hydrogenation of olefins, however, remains unresolved with respect to an analysis of all intervening intermediates and transition states.

3.3.1. Quantum Chemical Modeling of the Hydrogenation Mechanism

Two truncated systems were chosen for this study: $RuHCl(CO)(PH_3)_2$, an analogue of catalyst **1**,[25] and $RuHCl(PH_3)_3$, an analogue of $RuHCl(PPh_3)_3$.[44] $RuHCl(CO)(PH_3)_2$ and

$RuHCl(PH_3)_3$ were then used to model the dissociative mechanism for Ru-catalyzed hydrogenation, as outlined below.

(1) Phosphine dissociation occurs from Ru, generating a monophosphine species with a vacant coordination site *cis* to the hydride. For $RuHCl(PH_3)_3$, this process occurs preferentially, with dissociation of a PH_3 that is *trans* to another PH_3.

(2) Side-on approach of ethylene to the electron-deficient monophosphine complex results in the stabilizing formation of a Ru-ethylene adduct in which the olefin is π-bound to the metal centre.

(3) H_2 coordinates to the bottom face of the Ru-ethylene adduct and *trans* to the hydride.

(4) The Ru-H and H-H bonds elongate slightly, while the Ru-olefin and Ru-H_2 bonds shorten (TS1).

(5) Olefin insertion into the Ru-H bond generates the ethyl intermediate with coordinated H_2. The metal centre is stabilized by an agostic interaction with a hydrogen from the CH_3 portion of the ethyl ligand.

(6) The H-H bond elongates as one of the two hydrogens approaches the $-CH_2CH_3$ ligand (TS2).

(7) Two Ru-H bonds of high covalent character are formed.

(8) TS3 is generated and results in partial formation of a C-H bond.

(9) Ethane is eliminated and the active catalyst, $RuHCl(L)(PH_3)$ (L = CO or PH_3) is regenerated.

With respect to the intermediates, transition states and products formed, $RuHCl(CO)(PH_3)_2$ and $RuHCl(PH_3)_3$ follow identical reaction pathways. In each case, ethane is eliminated exergonically and the active catalyst [$RuHCl(L)(PH_3)$; L = CO or PH_3] is regenerated.

Therefore, the possibility that the activating effect of CO is due to some radical change in mechanism can be ruled out. The energetic consequences for ethene reduction by both model systems are shown below.

Table 3.3 Relative energies for ethene reduction catalyzed by $RuHCl(CO)(PH_3)_2$ and $RuHCl(PH_3)_3$.[a]

Step	ΔG (kcal mol^{-1})	
	CO	PH_3
Phosphine dissociation	15.8	14.4
Ethene coordination	5.9	5.4
H_2 Coordination	18.2	14.8
TS1	20.6	18.4
H_2 + ethyl intermediate	18.2	14.8
TS2	17.7	14.0
Cleaved H_2 + ethyl ground state	17.5	13.7
TS3	17.5	14.4
Active Catalyst + ethane	-10.6	-12.0

[a]All values are calculated using the B3LYP functional and the LACVP** basis set.

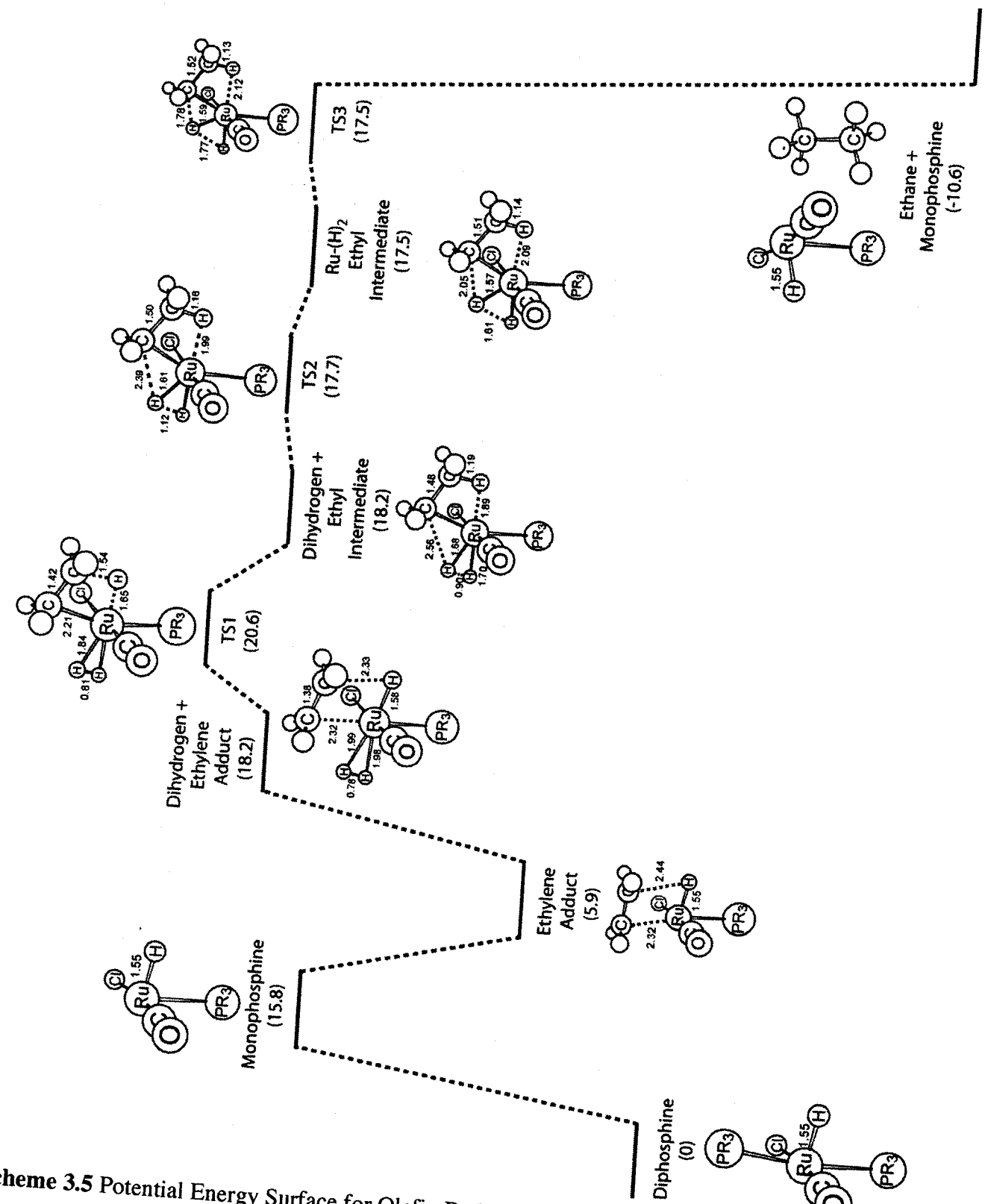

Scheme 3.5 Potential Energy Surface for Olefin Reduction by model system $RuHCl(CO)(PH_3)_2$.

Phosphine dissociation and ethylene coordination [(1) - (3)].

Phosphine dissociation occurs with approximately equal free energy (ΔG) for $RuHCl(CO)(PH_3)_2$ and $RuHCl(PH_3)_3$ (Table 3.3). The difference between the ΔG values for both systems, 1.2 kcal mol^{-1}, is approximately equal to the error in the computational method and is not chemically significant. The similarity in the values for the free energies for phosphine dissociation may be an artifact of the truncated PH_3-based model systems. As larger phosphines are incorporated, their steric bulk, as measured by cone angles, would be expected to increase the steric congestion at the metal centre. The experimentally-relevant ligands, PCy_3 and PPh_3, may be particularly vulnerable to this error (Table 3.4).

Table 3.4 Selected cone angles of representative phosphines.[48]

L	Cone Angle (deg.)
PH_3	87
PMe_3	118
PEt_3	132
PPh_3	145
PCy_3	170
$P(Bu^t)_3$	182

Dihydrogen coordination and adduct formation [(4) and (5)].

From the energetic profile for the reduction of ethane (Scheme 3.5), the coordination of H_2, which results in the dihydrogen + ethylene adduct, is the rate-limiting step. This is in agreement with the first-order dependence on H_2 and up to first-order dependence on olefin

implied in the rate law (Equation 3.1). This is consistent with the assumption of the "unsaturated" mechanism for hydrogenation (i.e. coordination of olefin prior to H_2), which has much precedent for neutral ruthenium hydrido complexes reducing simple alkenes.[5] Incoming H_2 binds to the bottom face of the ethene adduct and *trans* to the hydride ligand. Coordination of H_2 *trans* to a ligand of high *trans* influence (i.e. hydride), is well documented[49,50] and is driven by eventual formation of a stable octahedral complex.[51]

Coordination of H_2 results in lengthening of the Ru–H bond distance (Table 3.5), implying a reduction in the σ character of the Ru–H bond. TS1 reflects a structure that is intermediate between a Ru-hydride bond and a Ru–CH_2CH_2H agostic interaction. This observation is made based on the finding that for TS1 the Ru-H bond length is 1.65 Å while the distance between this hydrogen and the nearest carbon (from ethylene) is only 1.54 Å. The magnitude of this effect is approximately equal for $RuHCl(CO)(PH_3)_2$ and $RuHCl(PH_3)_3$, and it is therefore unrelated to the activating effect of the CO ligand.

Table 3.5 Changing length of the Ru–H bond following H_2 coordination.

Step	Ru–H (Å)	C–H (Å)
Ethylene adduct	1.55	2.44
Dihydrogen + ethene adduct	1.58	2.33
TS1	1.65	1.54
Dihydrogen + ethyl intermediate	1.89	1.19
TS2	1.99	1.16
Ru–$(H)_2$ + ethyl intermediate	2.09	1.14

Dihydrogen complexes, ruthenium-hydrogen bonds and ethane elimination [(6)-(10)].

A transient dihydrogen + ethyl intermediate undergoes facile elimination of ethane and regeneration of the active catalyst. The energy barriers between the dihydrogen + ethyl intermediate and TS2, TS2 and the Ru–$(H)_2$ + ethyl intermediate and between the Ru–$(H)_2$ + ethyl intermediate and TS3 are negligible, ranging from 0.2 kcal mol^{-1} to 0.5 kcal mol^{-1}. It is interesting to note, however, that the agostic interaction between the ruthenium and the proton on the $-CH_3$ end of the ethyl ligand weakens; the interaction length increases from 1.89 Å (dihydrogen + ethyl intermediate) to 2.09 Å (Ru–$(H)_2$ + ethyl intermediate), respectively (Figure 3.5). This implies that formation of two ruthenium-hydrogen bonds results in a net *increase* of electron density at the Ru centre, a finding that is further supported by natural population analysis (Table 3.6).

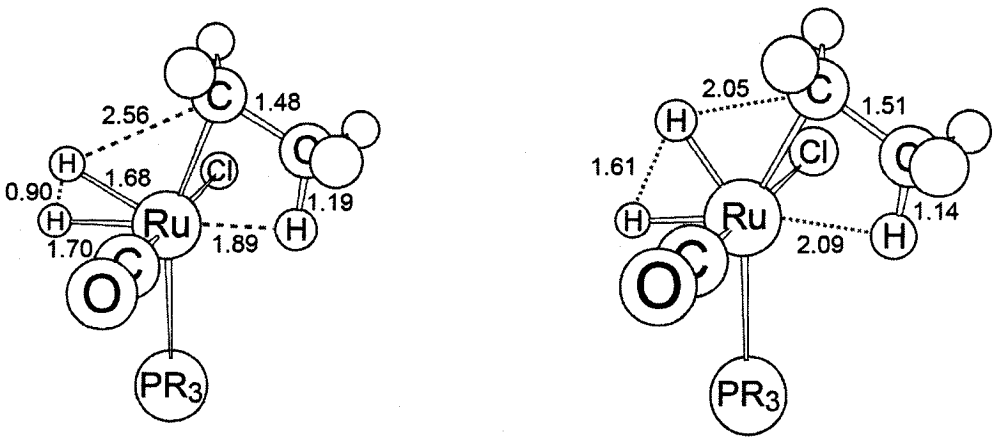

A **B**

Figure 3.5 A decrease in the Ru-ethyl agostic interaction is seen going from structure **A** to **B**.

Table 3.6 Natural population analysis of the dihydrogen + ethyl intermediate and the Ru–$(H)_2$ + ethyl intermediate.

Species	Natural Population Analysis Charge		
	Ru	H^a	H^a
Dihydrogen + ethyl intermediate	-0.303	0.145	0.136
Ru–$(H)_2$ + ethyl intermediate	-0.421	0.178	0.166

[a] Refers to a hydrogen atom from the coordinated molecule of H_2.

The charge on the Ru centre becomes more negative going from the dihydrogen + ethyl intermediate to the Ru–$(H)_2$ + ethyl intermediate (Table 3.6). The H atoms that originated from the coordinated molecule of H_2 and which become bonded to Ru, upon formation of the Ru–$(H)_2$ + ethyl intermediate, become more positive. These findings are consistent with a reduction of ruthenium and not the oxidation that would normally accompany formation of a classical ruthenium-hydride bond. Data from an examination of geometries belonging to the dihydrogen + ethyl and Ru–$(H)_2$ + ethyl intermediates (Figure 3.5) and an analysis of natural populations (Table 3.6) indicate that complete cleavage of the H–H bond does occur prior to ethane elimination. However, this dissociation results in formation of two covalent Ru–H bonds, rather than oxidation of the ruthenium centre and generation of two ionic Ru-H bonds.

CO bond length measurements during the catalytic cycle

The function of the CO ligand in ruthenium hydrido carbonyl complexes is unclear. The CO ligand may effectively destabilize the $Ru(H)_2$ intermediate, generated from H_2 activation, and increase the rate of alkane elimination. It may also stabilize the active catalyst towards olefin

coordination by making it more electron deficient. Finally, it may serve simply to stabilize the active catalyst against decomposition to an extent that a labile donor, such as H_2, cannot. If the CO ligand does exert a stabilizing/destabilizing effect at differing periods in the catalytic cycle, this should be reflected in its bond length (Figure 3.6). Donation would cause an increase in the C–O bond length, as electron density is polarized more towards the metal centre and, conversely, back-accepting electron density causes an elongation in the CO bond as electrons from filled metal orbitals are transferred into unfilled anti-bonding π^* orbitals on the CO.

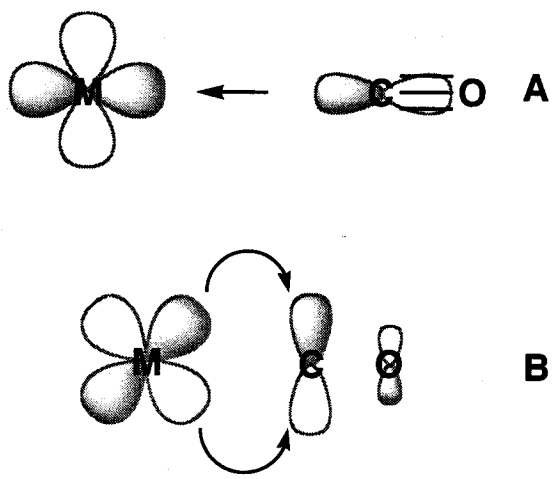

Figure 3.6 The carbon monoxide ligand is able to both donate (**A**) and accept (**B**) electron density from the metal centre.

For $RuHCl(CO)(PH_3)_2$, the C–O bond length is invariant throughout the catalytic cycle, implying that no back-donation from the metal to this ligand has occurred (Table 3.7). The Ru–C bond length, which would shorten if back-donation were occurring, is also invariant. No net stabilization of the rate-determining step for hydrogenation mediated by $RuHCl(CO)(PH_3)_2$ was seen, suggesting CO ligand incorporation does not have a beneficial kinetic effect on the reaction

rate. The foregoing data indicate that the activating effect of CO is not due to its ability to accept and donate electron density to and from the metal centre, as required, throughout the entire catalytic cycle.

Table 3.7 C–O and Ru–C bond lengths for model system $RuHCl(CO)(PH_3)_2$ and Ru-P bond lengths for model system $RuHCl(PH_3)_3$.

Species	Bond Length (Å)	
	C–O	Ru–C
Diphosphine	1.161	1.869
Monophosphine	1.159	1.881
Ethylene Adduct	1.160	1.869
Dihydrogen + ethylene adduct	1.158	1.876
TS1	1.158	1.880
Dihydrogen + ethyl intermediate	1.159	1.885
TS2	1.156	1.886
Dihydride + Ethyl Intermediate	1.156	1.883
TS3	1.157	1.882

Computational data do not support the proposal that the presence of a carbonyl ligand in a ruthenium hydride catalyst activates the complex toward hydrogenation of olefins. However, an alternative, and as yet untested, explanation for the effect of this ligand is proposed based on a steric arguments. Olefin approach to the coordinatively-unsaturated active catalyst is more favoured for CO-containing systems: carbon monoxide is a planar 2-electron donor while the steric demand imposed by phosphine ligands can be significant, possibly blocking alkene coordination. Catalyst decomposition may also be prevented by the CO ligand to an extent that a labile donor, such as H_2, cannot.

3.4 Conclusions

Incorporation of *N*-heterocyclic carbenes into catalyst systems with labile ancillary ligands has mixed effects on catalyst activity and performance. $RuHCl(CO)(IMes)(PPh_3)$ and $RuHCl(CO)(H_2IMes)(PPh_3)$ possess superior activity for the hydrogenation of sterically-hindered and *trans* internal olefins, relative to $RuHCl(CO)(PCy_3)_2$ and $RuHCl(CO)(IMes)(PCy_3)$. The poor reactivity of **2** is worth noting: the presence of a labile phosphine donor in the pre-catalyst is clearly essential to activity of the N-heterocyclic carbene complexes and is consistent with the requirement for dissociation of a neutral donor ligand. The increased isomerization and polymerization tendencies exhibited by **3** and **4** detracts from their potential as hydrogenation catalysts for isomerizable double bonds or for unsaturated cyclic substrates of low ring strain.

The origin of a possible activating effect afforded by incorporation of a carbonyl ligand into a ruthenium hydride catalyst remains unexplained. By monitoring CO bond lengths at various stages in the catalytic cycle, it was determined that CO does not act as an electron reservoir, donating or back-accepting electron density on demand. In addition, no net stabilization of the rate-limiting step by the CO-containing systems was seen. As an alternate possibility, it is proposed that incorporation of a CO ligand would reduce steric congestion at the metal centre, permitting facile olefin coordination.

3.5 References

(1) Pearson, R. G. *Acc. Chem. Res* **1971**, *4*, 152.

(2) James, B. R. *Homogeneous Hydrogenation*, John Wiley & Sons: Toronto, 1973.

(3) Ertl, G.; Knoezinger, H.; (Eds.) *Handbook of Heterogeneous Catalysis*, Wiley-VCH: Weinheim, Germany, 1997.

(4) Young, J. F.; Osborn, J. A.; Jardine, F. H.; Wilkinson, G. *Chem. Commun.* **1965**, 131.

(5) Chaloner, P. A.; Esteruelas, M. A.; Joo, F.; Oro, L. A. *Homogeneous Hydrogenation*, Kluwer: Boston, 1994.

(6) Zhang, W.; Jacobsen, E. N. *Tetrahedron Lett.* **1991**, *32*, 1711.

(7) Crabtree, R. H.; Demou, P. C.; Eden, D.; Mihelcic, J. M.; Parnell, C. A.; Quirk, J. M.; Morris, G. E. *J. Am. Chem. Soc.* **1982**, *104*, 6994.

(8) James, B. R., Comprehensive Organometallic Chemistry. In *Comprehensive Organometallic Chemistry*, Vol. 8, Chapter 51, and references therein, Wilkinson, G., Ed. Pergamon Press: New York, 1982.

(9) Naota, T.; Takaya, H.; Murahashi, S.-I. *Chem. Rev.* **1998**, *98*, 2599.

(10) Dinger, M. B.; Mol, J. C. *Organometallics* **2003**, *22*, 1089.

(11) Dharmasena, U. L.; Foucault, H. M.; dos Santos, E. N.; Fogg, D. E.; Nolan, S. P. *Organometallics* **2005**, *24*, 1056.

(12) Yi, C. S.; Lee, D. W. *Organometallics* **1999**, *18*, 5152.

(13) Lee, H. M.; Smith, D. C., Jr.; He, Z.; Stevens, E. D.; Yi, C. S.; Nolan, S. P. *Organometallics* **2001**, *20*, 794.

(14) Nkosi, B. S.; Coville, N. J.; Albers, M. O.; Gordon, C.; Viney, M. M.; Singleton, E. *J. Organomet. Chem.* **1990**, *386*, 111.

(15) Drouin, S. D.; Amoroso, D.; Yap, G. P. A.; Fogg, D. E. *Organometallics* **2002**, *21*, 1042.

(16) Ohkuma, T.; Takeno, H.; Honda, Y.; Noyori, R. *Adv. Synth. Catal* **2001**, *343*, 369.

(17) Geldbach, T. J.; Pregosin, P. S. *Helv. Chim. Acta* **2002**, *85*, 3937.

(18) Burling, S.; Whittlesey, M. K.; Williams, J. M. J. *Adv. Synth. Catal* **2005**, *347*, 591.

(19) Fogg, D. E.; James, B. R.; Kilner, M. *Inorg. Chim. Acta* **1994**, *222*, 85.

(20) Borowski, A. F.; Sabo-Etienne, S.; Donnadieu, B.; Chaudret, B. *Organometallics* **2003**, *22*, 1630.

(21) Borowski, A. F.; Sabo-Etienne, S.; Donnadieu, B.; Chaudret, B. *Organometallics* **2003**, *22*, 4803.

(22) Rosales, M.; Alvarado, Y.; Boves, M.; Rubio, R.; Soscun, H. *Transition Met. Chem.* **1995**, *20*, 246.

(23) James, B. R. *Advances in Organometallic Chemistry: Catalysis and Organic Syntheses*, 17, Academic: New York, NY, 1979.

(24) McManus, N. T.; Rempel, G. L. *J. Macromol. Sci., Rev. Macromol. Chem. Phys.* **1995**, *C35*, 239.

(25) (a) Yi, C. S.; Lee, D. Y. *Organometallics* **1999**, *18*, 5152. (b) Yi, C. S.; Lee, D. W.; He, Z. *Organometallics* **2000**, *19*, 2909.

(26) Martin, P.; McManus, N. T.; Rempel, G. L. *J. Mol. Catal. A* **1997**, *126*, 115.

(27) Diggle, R. A.; Macgregor, S. A.; Whittlesey, M. K. *Organometallics* **2004**, *23*, 1857.

(28) Sanford, M. S.; Love, J. A.; Grubbs, R. H. *J. Am. Chem. Soc.* **2001**, *123*, 6543.

(29) Vaska, L.; Rhodes, R. E. *J. Am. Chem. Soc.* **1965**, *87*, 4970.

(30) James, B. R. *Inorg. Chim. Acta, Rev.* **1970**, *4*, 73.

(31) Drouin, S. D. **2003**, Ph.D. Thesis, University of Ottawa.

(32) Rodriguez, V.; Sabo-Etienne, S.; Chaudret, B.; Thoburn, J.; Ulrich, S.; Limbach, H.-H.; Eckert, J.; Barthelat, J.-C.; Hussein, K.; Marsden, C. J. *Inorg. Chem.* **1998**, *37*, 3475.

(33) (a) Nkosi, B. S.; Coville, H. J.; Albers, M. O.; Gordon, C.; Viney, M.; Singleton, E. *J. Organomet. Chem.* **1990**, *386*, 111. (b) Fogg, D. E.; James, B. R.; Kilner, M. *Inorg. Chim. Acta* **1994**, *222*, 85. (c) Zanetti, N. C.; Spindler, F.; Spencer, J.; Togni, A.; Rihs, G. *Organometallics* **1996**, *15*, 860. (d) Bianchini, C.; Barbaro, P.; Scapacci, G.; Zanobini, F. *Organometallics* **2000**, *19*, 2450.

(34) Dinger, M. B.; Mol, J. C. *Eur. J. Inorg. Chem.* **2003**, 2827.

(35) Blaser, H.-U.; Malan, C.; Pugin, B.; Spindler, F.; Steiner, H.; Studer, M. *Adv. Synth. Catal* **2003**, *345*, 103.

(36) Perry, M. C.; Cui, X. H.; Powell, M. T.; Hou, D. R.; Reibenspies, J. H.; Burgess, K. *J. Am. Chem. Soc.* **2003**, *125*, 113.

(37) (a) Fürstner, A.; Langemann, K. *Synthesis* **1997**, 792-803. (b) Jafarpour, L.; Heck, M.-P.; Baylon, C.; Lee, H. M.; Mioskowski, C.; Nolan, S. P. *Organometallics* **2002**, *21*, 671. (c) Fürstner, A.; Ackermann, L. *Chem. Commun.* **1999**, 95. (d) Fürstner, A.; Langemann, K. *J. Org. Chem.* **1996**, *61*, 3942. (e) Fürstner, A.; Thiel, O. R.; Ackermann, L.; Schanz, H.-J.; Nolan, S. P. *J. Org. Chem.* **2000**, *65*, 2204. (f) Fürstner, A.; Langemann, K. *J. Am. Chem. Soc.* **1997**, *119*, 9130.

(38) Louie, J.; Bielawski, C. W.; Grubbs, R. H. *J. Am. Chem. Soc.* **2001**, *123*, 11312.

(39) Fogg, D. E.; dos Santos, E. N. *Coord. Chem. Rev.* **2004**, *248*, 2365.

(40) McLain, S. J.; McCord, E. F.; Arthur, S. D.; Hauptman, E.; Feldman, J.; Nugent, W. A.; Johnson, L. K.; Mecking, S.; Brookhart, M. *Poly. Mater. Sci. Eng.* **1997**, *76*, 246.

(41) Bielawski, C. W.; Morita, T.; Grubbs, R. H. *Macromolecules* **2000**, *33*, 678.

(42) G. Rousseau, *Tetrahedron* **1995**, *51*, 2777.

(43) (a) Bourgeois, D.; Pancrazi, A.; Nolan, S. P.; Prunet, J. *J. Organomet. Chem.* **2002**, *643-644*, 247. (b) Cadot, C.; Dalko, P. I.; Cossy, J. *Tetrahedron Lett.* **2002**, *43*, 1839. (c) Kinderman, S. S.; van Maarseveen, J. H.; Schoemaker, H. E.; Hiemstra, H.; Rutjes, F. P. J. T. *Org. Lett.* **2001**, *3*, 2045.

(44) Hallman, P. S.; McGarvey, B. R.; Wilkinson, G. *J. Chem. Soc. A* **1968**, 3143.

(45) Heyn, R. H.; Macgregor, S. A.; Nadasdi, T. T.; Ogasawara, M.; Eisenstein, O.; Caulton, K. G. *Inorg. Chim. Acta* **1997**, *259*, 5.

(46) Gerard, H.; Eisenstein, O. *J. Chem. Soc., Dalton Trans.* **2003**, 839.

(47) Gusev, D. G.; Kuhlman, R. L.; Renkema, K. B.; Eisenstein, O.; Caulton, K. G. *Inorg. Chem.* **1996**, *35*, 6775.

(48) Tolman, C. A. *Chem. Rev.* **1977**, *77*, 313.

(49) Marchenko, A. V.; Huffman, J. C.; Valerga, P.; Tenorio, M. J.; Puerta, M. C.; Caulton, K. G. *Inorg. Chem.* **2001**, *40*, 6444.

(50) Maseras, F.; Lledos, A.; Clot, E.; Eisenstein, O. *Chem. Rev.* **2000**, *100*, 601.

(51) Riehl, J. F.; Jean, Y.; Eisenstein, O.; Pelissier, M. *Organometallics* **1992**, *11*, 729.

CHAPTER 4

Tandem Application of ^{1}H PGSE and ^{31}P Solid-State NMR Techniques to Resolve Ambiguities in Nuclearity of a Chelate-Sabilized Ruthenium (σ-Pyrrolato) Complex

4.1. Introduction

As part of an ongoing effort in the Fogg group to develop pseudohalide ligands for use in Ru-mediated olefin metathesis,[1] the design of catalysts containing a chelating N-anionic donor was pursued.[2] A potential limitation of monodentate ligands of this type is the tendency toward π-coordination of the heterocyclic ring to give piano-stool complexes. This transformation has been previously documented for transition metal complexes of phenoxide ligands, and is discussed in Chapter 1.

Preliminary studies focused on chelating ligands containing a pyrrolato and an imine group. Iminopyrrolato complexes **9a** and **9b** promoted both ring-closing metathesis and ring-opening metathesis polymerization in air and in non-degassed solvents. Catalytic activities of these compounds were impaired due to both the absence of an electron-donating ligand in the metathesis-active intermediate and the low lability of PCy_3 and pyridine. An elevated reaction temperature (70 °C) was required to induce metathesis via **9a** and **9b**.[2]

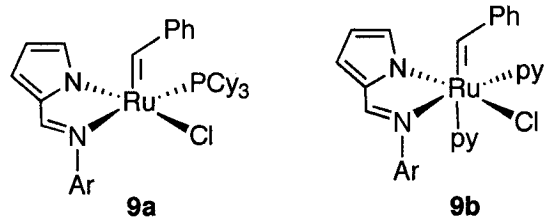

9a **9b**

Figure 4.1 Metathesis-active σ-bound pyrrolide complexes of ruthenium [Ar = 2,6-^{i}Pr-C_6H_3].

σ→π Isomerization of the pyrrolide arm of the iminopyrrolato ligand may provide a deactivation pathway that competes with metathesis (Scheme 4.1). Both reactions are initiated by loss of a phosphine, with subsequent olefin coordination propagating metathesis (path **A**). Competing σ→π isomerization of the pyrrolide ring deactivates the catalyst, ultimately generating an 18-electron species whose coordinative saturation would preclude additional olefin coordination (path **B**).

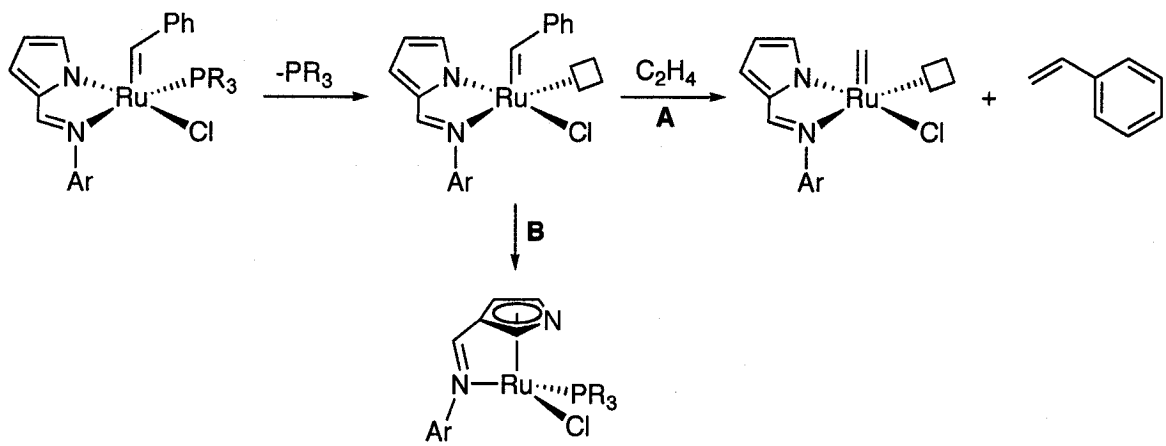

Scheme 4.1 The relationship between metathesis (**A**) and σ→π isomerization (**B**) [Ar = 2,6-^{i}Pr-C_6H_3; R = Cy].

π-Pyrrolides are common in transition metal chemistry[3-5] and include ruthenium derivatives.[6] The chelating 2-[(2,6-diisopropylphenyl)imino]pyrrolide ligand may favour σ-coordination, however, given its narrow bite angle of 70-85°[7-12] and the thermodynamic stability of the five-membered chelate ring. Earlier work from the Fogg group (Equations 4.1 and 4.2) demonstrate that use of small (five or six-membered) chelate rings give stable σ-aryloxide ligands, though larger more flexible seven-membered chelates rapidly isomerize.[13,14]

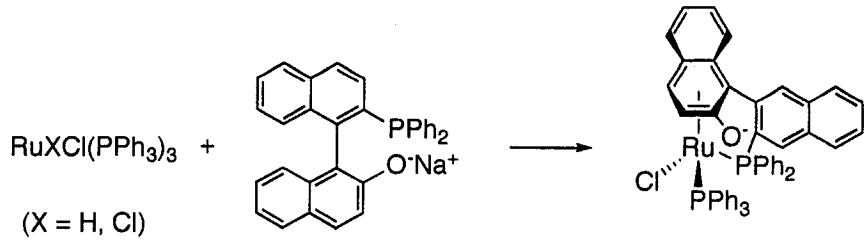

(4.1)

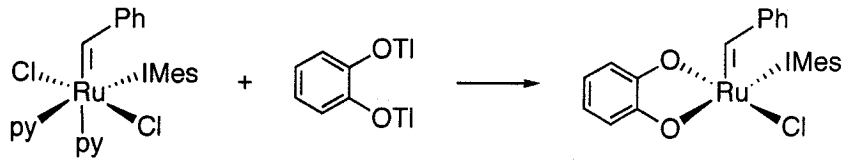

(4.2)

Nevertheless, it remained unclear whether the stability of the σ-bound pyrrolide group in **9a** and **9b** was a true reflection of the favoured coordination mode of the ligand, or whether it was an artifact of the low lability of the ancillary PCy_3 and pyridine ligands. Loss of PCy_3 or pyridine would be required to generate the three coordination sites needed for π-coordination. In order to examine this point directly, reaction of $RuCl_2(PPh_3)_3$ with the iminopyrrolide ligand was undertaken. This would permit direct comparison with the corresponding reaction of the pyrrolide itself.

4.2. Synthesis of $[RuCl(\kappa^2\text{-}N,N'\text{-}ArN{=}CHC_4H_3N)(PPh_3)_2]_x$

Reaction of $RuCl_2(PPh_3)_3$ (**5**) with 1.8 equivalents of lithium 2-[(2, 6-diisopropylphenyl)imino]pyrrolide (**7**) in dichloromethane effected conversion to a single product of empirical formula $[RuCl(\kappa^2\text{-}N,N'\text{-}ArN{=}CHC_4H_3N)(PPh_3)_2]_x$ (**8**) in 12 h at room temperature as determined by in situ $^{31}P\{^1H\}$ NMR analysis (Scheme 4.2). The requirement for excess LiNN', established in earlier work by Samantha Drouin of this research group,[2] was due

to competing protonation of the ligand (giving 2-{(2, 6-$^{i}Pr_2C_6H_3$)-N=CH}C_4H_4N, **6**) by deprotonation of the reaction solvent. Isolated yields of **8** were limited to 72 % by high solubility in all hydrocarbon solvents, including pentane.

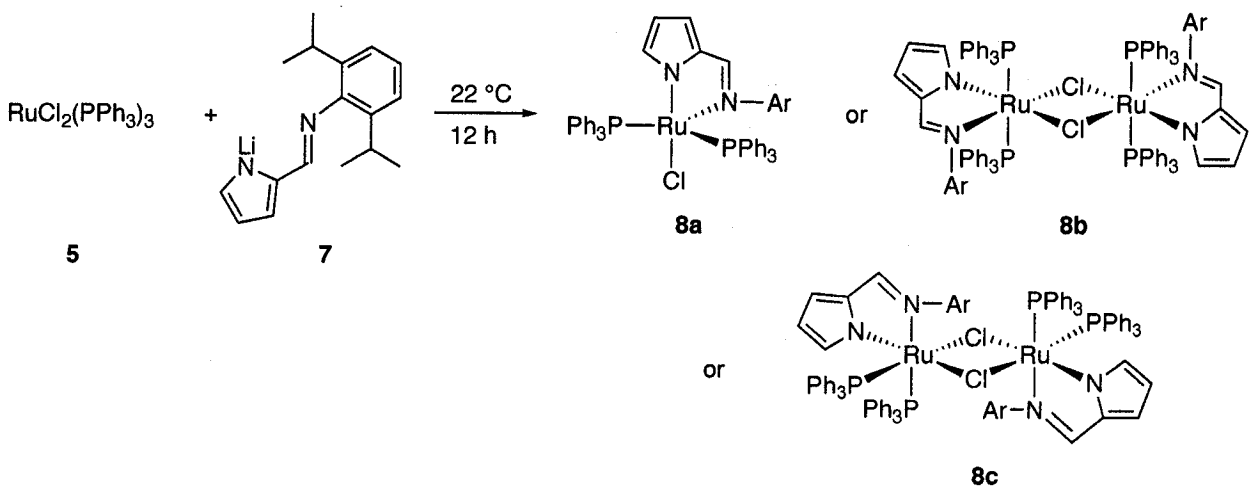

Scheme 4.2 Preparation of Ru-iminopyrrolato complex **8** [Ar = 2,6-^{i}Pr-C_6H_3].

4.2.1. Molecular Structure of 8

In order to establish the coordination mode of the iminopyrrolide ligand, a series of two-dimensional NMR experiments (^{1}H COSY, ^{1}H-^{13}C HMQC, ^{1}H-^{13}C HMBC) were performed. This enabled full assignment of the ^{1}H and $^{13}C\{^{1}H\}$ NMR spectra. Resonances due to the pyrrolide arm of the ligand were deconvoluted from those due to the aromatic portion and from those due to triphenylphosphine. Using the azomethine proton as a starting point, the resonances due to C2 and C3 were located by ^{1}H-^{13}C HMBC experiments. C2 and C3 were differentiated on the basis of the C3-H3 coupling observed in the HMQC spectrum. In turn, this permitted location of H4 (COSY) and C4 (HMQC) and subsequent location of H5 (COSY) and C5 (HMQC).

Chemical shifts for the pyrrolide ring in **8** (δ_H 7.15, 6.34 and 6.18 ppm and δ_C 147.5, 143.7 and 121.3 ppm) fall within the established range for a σ-coordinated anionic pyrrole ring[7,8,10,12] and differ only slightly from values corresponding to the parent lithium salt. ^1H and ^{13}C chemical shifts provide a good indicator for the coordination mode of the pyrrolide ring; differences in ^1H and ^{13}C chemical shifts for σ and π coordinated pyrrolides are about 1-2 ppm and 30 ppm, respectively, with the latter values lying upfield (Table 4.1).

Table 4.1 Key NMR data for the pyrrolyl group.[a]

Compound	Solvent	^{1}H NMR	^{13}C NMR	Ref.
HNN'	C_6D_6	6.45 (br, 1 H), 6.05 (br, 2 H)	150.7, 115.9	7,15
LiNN'	C_6D_6	7.15-7.2 (m, 1H), 6.89 (m, 1 H), 6.42 (m, 1 H)	147.5, 120.7	2,7
9a	$CDCl_3$	7.09 – 7.01 (***H5***, overlaps with Ar), 6.51 (br, 1 H, ***H3***), 6.18 (dd, $^3J_{HH}$ = 3.9, 1.6 Hz, 1 H, ***H4***)	142.8 (d, $^3J_{CP}$ = 2.0 Hz, ***C2***), 141.7 (s, ***C3***), 120.2 (s, ***C5***), 114.0 (s, ***C4***)	2
9b	$CDCl_3$	8.59 – 6.91 (***H5***, overlaps with Ar), 6.46 (br, 1 H, ***H3***), 6.20 (m, 1 H, ***H4***)		2
$RuCl(\mu^5\text{-}C_5H_4N)(PPh_3)_2$	C_6D_6	5.61 (2H), 4.24 (2H)	108.4, 82.7	6
$RuH(\mu^5\text{-}C_5H_4N)(PPh_3)_2$	C_6D_6	5.33 (2H), 5.03 (2H)	110.0, 82.0	6
8	C_6D_6	7.15 (br s, 1 H, ***H5***), 6.34 (m, 1 H, ***H4***), 6.18 (br m, 1 H, ***H3***)	147.5 (s, ***C2***), 143.7 (s, ***C3***), 121.3 (s, ***C5***), 114.5 (s, ***C4***)	This work

[a] Chemical shifts are reported in ppm. Coupling constants are given in Hz. Assignments (where reported) are shown in bold face.

The presence of two triphenylphosphine ligands per Ru centre is inferred from observation of the triplet multiplicity of the azomethine proton resonance (δ 7.90 ppm, $^4J_{HP}$ = 2.1 Hz), which collapses to a singlet upon proton decoupling. The presence of a sharp singlet was noted in the $^{31}P\{^1H\}$ spectrum of **8** (δ 58.5 ppm). Data from both the ^1H and ^{31}P NMR experiments provide strong evidence for the presence of two equivalent, *trans*-disposed triphenylphosphine ligands, as shown in structure **8b**. Inconsistent with this geometry, however, are data from a variable-temperature ^{31}P NMR experiment conducted in toluene-d_8 (m.p. -93 °C) (Figure 4.2). Spectra were collected in increments of –10 °C from 20 °C to -90 °C. The signal decoalesced at -70 °C, and partial resolution into two broad signals at 71.8 ppm and 46.8 ppm was unexpectedly achieved at -90 °C (the average of these two resonances, 59.3 ppm, is approximately equal to the location of the singlet at room temperature, 58.5 ppm). This behavior indicates that the phosphorus centres are inequivalent, ruling out structure **8b**. The breadth and singlet multiplicity of these resonances ($\upsilon_{0.5}$ = 110 Hz and 99 Hz, respectively) implies rapid interconversion of the inequivalent phosphorus centres even at -90 °C. Arguing against dissociation and re-coordination of the triphenylphosphine ligands as a mechanism for this interconversion, ^{31}P EXSY experiments performed at room temperature and -90 °C in the presence of a five-fold excess of triphenylphosphine show no correlation between the free and bound ligand. This suggests that the mechanism for exchange of the inequivalent triphenylphopshine ligands is due to conformational flexibility in **8**.

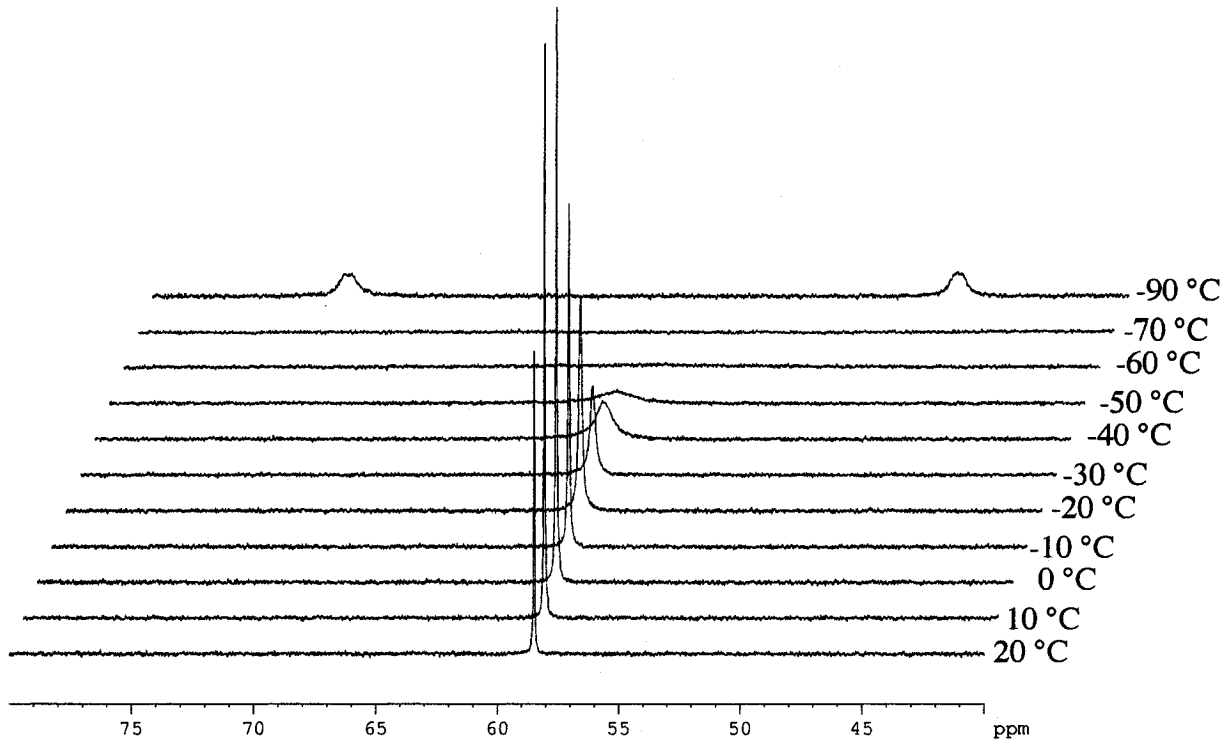

Figure 4.2 $^{31}P\{^{1}H\}$ Variable-temperature NMR analysis of **8**.

To further examine the consequences of the analysis shown in Figure 4.2, **8** was subjected to solid-state NMR analysis. Justification for this analysis comes from the realization that the fast exchange of the inequivalent triphenylphosphine ligands, which causes the signal averaging mentioned above, is mediated by solvation. Observation of **8** in the solid state (where such a process would be frozen out) should permit unequivocal determination of the absolute orientation of the triphenylphosphine ligands (i.e. *cis* or *trans*-disposed).

4.3. Determining Absolute Ligand Orientation in 8 by Solid State NMR

4.3.1. Theoretical Background

Relative to solution NMR spectra, spectra recorded in the solid state appear broad and less resolved and typically require longer acquisition times. The reasons for these differences

include: the presence of orientation-dependent parameters normally averaged out in solution due to molecular tumbling, and the existence of longer spin-lattice relaxation times due to sample rigidity.

Dipolar coupling (D_C), an orientation-dependent parameter, arises from the interaction between nuclear magnetic moments of two nuclei.[16] Each nucleus produces a small magnetic field due to its own rotation. Adjacent nuclei separated by less than 10 Å have the potential to greatly affect the effective local magnetic field or resonance frequency of a neighbouring nucleus. This is the dominant interaction between nuclei in the solid state. D_C coupling is on the order of 1×10^2 to 1×10^4 Hz[17] and can obscure observation of through-bond J couplings and even chemical shifts, resulting in broadened signals. The magnitude of dipolar coupling is dependent on two main factors (Figure 4.3): the internuclear distance (r), where D_C is inversely proportional to r^3, and the internuclear vector, the orientation of which is governed by the term $3\cos^2\theta - 1$, and where θ is the angle between the vector and B_o.[16] A polycrystalline sample, such as **8**, would produce a spectrum composed of a statistical distribution of resonances representing all possible orientations of the internuclear vector. At the magic angle, when $\theta = 54.74°$ (i.e. $3\cos^2\theta - 1 = 0$), the resonance is completely unperturbed by through-space interactions with nearby dipoles.

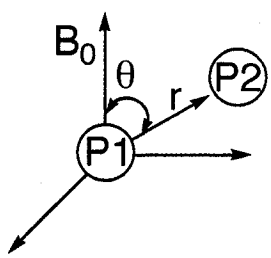

Figure 4.3 Dipolar coupling between two ^{31}P nuclei (P1 and P2) at a distance r apart, oriented at an angle θ with respect to the external magnetic field (B_o).

Another orientation-dependent parameter is the chemical shift anisotropy. Electrons are perturbed, albeit to a lesser extent, by the application of an external magnetic field (B_o). Therefore, the effective magnetic field felt by a given nucleus is perturbed not only by spin-spin (J) and dipolar coupling (D_C) but also by the orbiting electrons in the order, $J << D_C \approx$ chemical shift anisotropy. This latter parameter is highly dependent on the symmetry of the electron cloud and, because this symmetry is rarely spherical, the effect of its orientation with respect to B_o varies as a result of its non-uniform shape.[16,18]

When the narrowest part of the electron cloud is oriented parallel to B_o, the largest chemical shift, or most de-shielded resonance, is observed. The opposite is true for the widest part of the electron cloud. These represent the extremes of shielding and are denoted δ_{11} and δ_{33}, respectively. Orientation of the electron cloud perpendicular to δ_{11} and δ_{33} is denoted by δ_{22} (Figure 4.4) and $\delta_{11} \geq \delta_{22} \geq \delta_{33}$. These three quantities constitute the principal elements of the chemical shift tensor, and provide insight into molecular structure and bonding. Their effect on a nucleus is dependent on the angle (θ) that the principal axis of the electron cloud makes to B_o. At the magic angle ($\theta = 54.74°$), the term describing the angular dependence of the chemical shift ($3\cos^2\theta - 1$) becomes zero. The effects of anisotropy are thus nullified. This leaves only the isotropic chemical shift which corresponds to the averaged chemical shift that is observed in solution, with minor deviations arising from solvent effects and crystal packing.[19]

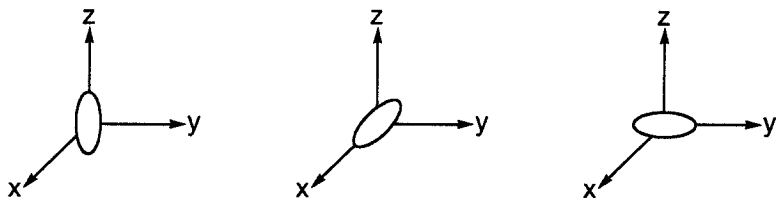

Figure 4.4 The principal shielding components of the chemical shift tensor δ_{11}, δ_{22} and δ_{33}, respectively.

Spinning a powdered sample inside the spectrometer at 54.74° relative to B_0, a technique called Magic Angle Spinning (MAS),[20,21] nulls the effects of both dipolar coupling and inhomogenities in the shape of the anisotropic chemical shift ellipsoid. Both of these phenomena can obscure observation of the isotropic chemical shift. At a certain threshold spinning frequency, with the sample oriented at the magic angle relative to B_0, only the isotropic chemical shifts of a sample are observed. Below this level, resonances appear at integer multiples of the spinning frequency.[20,21] Called 'spinning sidebands', these result from incomplete averaging of the chemical shift anisotropy, and can provide the principal elements of the chemical shift tensor. The number of these sidebands increases as the spinning speed decreases.

The second major obstacle to overcome when measuring NMR spectra in the solid state is the increase in spin-lattice relaxation times, which results in lower signal-to-noise ratios. Phosphorus-31, the nucleus of interest in this study, is 100 % abundant and spin 1/2 active, with a natural sensitivity of 0.0665 (relative to ^{1}H at 1.00 and ^{13}C at 0.0159).[22] In general, the number of ^{31}P nuclei to be observed in a given sample is low, resulting in low signal intensities. Therefore, to reduce acquisition times and produce better resolved spectra, it becomes necessary to indirectly increase the signal intensity for ^{31}P using a technique called cross-polarization

(CP).[23] Cross polarization[24-26] transfers magnetization from ^{1}H, a nucleus highly receptive to magnetization, to the nucleus under study as shown in the pulse sequence in Scheme 4.3.

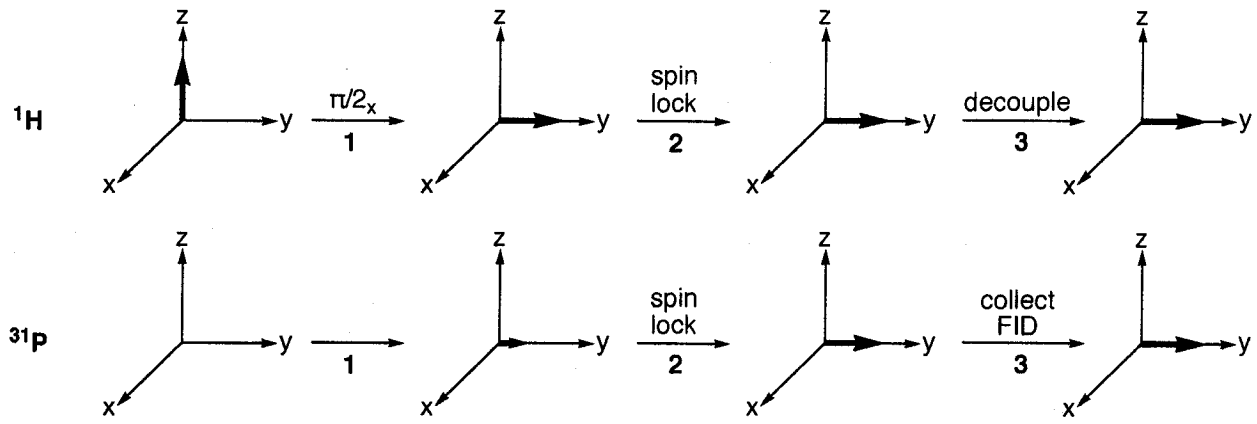

Scheme 4.3 Simplified pulse sequence for cross polarization. The bolded arrow represents the magnetization vector of the sample.

^{1}H magnetization is transferred onto the *y*-axis by a $\pi/2$ (**1**) pulse and a continuous pulse is then applied to keep its magnetization precessing about this axis (**2**). Once the ^{31}P channel, for example, is turned on, a pulse is applied at the same frequency as the resonating protons (*the Hartmann-Hahn condition*[27]) and both nuclei are spin-locked (**2**). During this contact period, magnetization is transferred from ^{1}H to ^{31}P by dipolar coupling, magnifying the signal intensity for the ^{31}P nucleus. The final step is collection of the ^{31}P free induction decay and decoupling of the protons (**3**). Through the simultaneous application of magic angle spinning (MAS) and cross-polarization (CP), abbreviated as CP-MAS NMR, highly resolved experiments with dramatically reduced acquisition times are possible. It is this technique that forms the basis for the solid state NMR experiments discussed below.

4.3.2. One Dimensional $^{31}P\{^{1}H\}$ CP-MAS NMR

As seen in Figure 4.5, two signals are visible in the room temperature solid state spectrum of **8**, with isotropic chemical shifts equal to 66.8 ppm and 52.1 ppm. This observation indicates the presence of two magnetically-inequivalent ^{31}P sites in the asymmetric unit cell of the crystal structure. The average of the signals seen in the solid state, 59.5 ppm, corresponds to the singlet at 58.5 ppm in the room temperature solution state spectrum. The isotropic chemical shifts are flanked by spinning side bands at integer multiples of the spinning frequency, which span about 200 ppm. This suggests substantial anisotropy in the ^{31}P chemical shift tensor (*vide infra*).

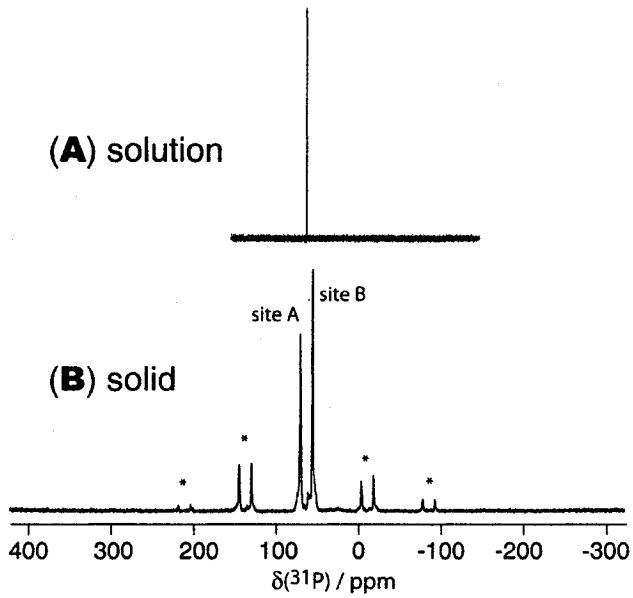

Figure 4.5 $^{31}P\{^{1}H\}$ NMR spectra of **8c** (22 °C) (**A**) Solution spectrum (C_6D_6, 7.05 T) (**B**) Solid-state CP/MAS spectrum (4.7 T; MAS rate = 5.3 kHz). Pairs of spinning sidebands are marked with asterisks. Fine structure at the base of these peaks is due to $J(^{99}Ru, ^{31}P)$ coupling.

4.3.3. Evidence for ^{31}P Coupling to ^{99}Ru

The bases of peaks seen in Figure 4.5 reveal fine splitting due to $^{1}J(^{31}P\text{-}^{99}Ru)_{iso}$ coupling. A more detailed spectrum was constructed by adding in the intensities of the spinning sidebands for the resonance centered at 66.8 ppm (site "A") (Figure 4.6). The predominant peak, at 66.8 ppm, is due to ^{31}P nuclei next to spin-0 Ru isotopes (^{96}Ru, ^{98}Ru, ^{100}Ru, ^{102}Ru, ^{104}Ru).[28] The fine structure is due to ^{31}P coupling to ^{99}Ru (12.8 % abundant, I = 5/2)[28] and consists of 6 peaks with the difference between the highest and lowest field signals (1218 Hz) being five times the isotropic $J(^{31}P, ^{99}Ru)$ coupling constant. This makes $^{1}J(^{31}P, ^{99}Ru)$ equal to 244 Hz, which represents one of the largest of such values reported for an Ru-P bond.[29] Due to the self-decoupling of ^{101}Ru (I = 5/2) from ^{31}P, no coupling occurs between these two nuclei. This can be traced to the larger nuclear electric quadrupole moment of ^{101}Ru relative to ^{99}Ru ($Q(^{101}Ru)/Q(^{99}Ru) = 5.78$.

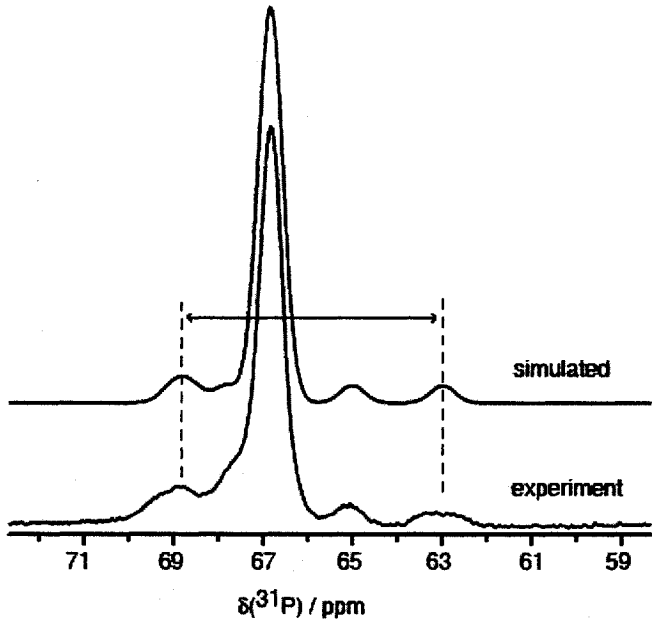

Figure 4.6 Solid-state ^{31}P CP/MAS NMR centreband of one of the two ^{31}P sites in **8c** (11.75 T; all sidebands summed into the centreband to approximate an infinite-MAS-rate spectrum). The simulated spectrum is generated using the parameters summarized in Table 4.2.

Details concerning simulation of a spectrum of a spin-1/2 nucleus (^{31}P) coupled to a half-integer quadrupolar nucleus (^{99}Ru) are discussed in the literature.[30] Observation of residual dipolar coupling (d_C), coupling between ^{31}P and ^{99}Ru that is not totally averaged out by MAS, is due to the effect of the quadrupolar interaction parameter on the quadrupolar nucleus. The magnitude of this effect was measured and is equal to -140 Hz (at 11.75 T). This value is, in turn, dependent on the quadrupolar coupling constant ($C_q(^{99}Ru)$), the asymmetry parameter of the electric field gradient (EFG) tensor, the effective dipolar coupling constant (^{99}Ru-^{31}P), the orientation of the dipolar vector relative to the EFG tensor (described by angles α, β) and the Larmor frequency.

The electronic structure of **8c** was probed further by conducting ^{31}P dipolar chemical shift experiments[31] at two different field strengths (Figure 4.7). The resulting spectra provide information about the ^{31}P chemical shift tensors, and their orientation relative to the ^{31}P-^{31}P dipolar vector. It is assumed that the ^{31}P spin systems are effectively isolated and do not couple with spin-active isotopes of Ru or Cl. The good agreement between the simulated and observed spectra in Figure 4.7 supports this assumption. The effective ^{31}P-^{31}P dipolar coupling constant was 660 ± 50 Hz, from which a through-space ^{31}P-^{31}P separation of about 3.1 Å was calculated. Trans-disposed phosphine ligands, on the other hand, have a through-space ^{31}P-^{31}P separation of about 4.6 Å, or twice the equilibrium Ru-P bond length.[13] This permits exclusion of **8b** as a possible structure. Cisoid triphenylphosphine ligands have a through-space ^{31}P-^{31}P separation of 4.0 Å,[32] which is larger than the calculated value of 3.1 Å for compound **8**. This then allows exclusion of structure **8a**, where the triphenylphosphines are cisoid, as a possible structure for **8**. Therefore, compound **8** is best represented by structure **8c**, where the triphenylphosphine ligands are *cis*-disposed.

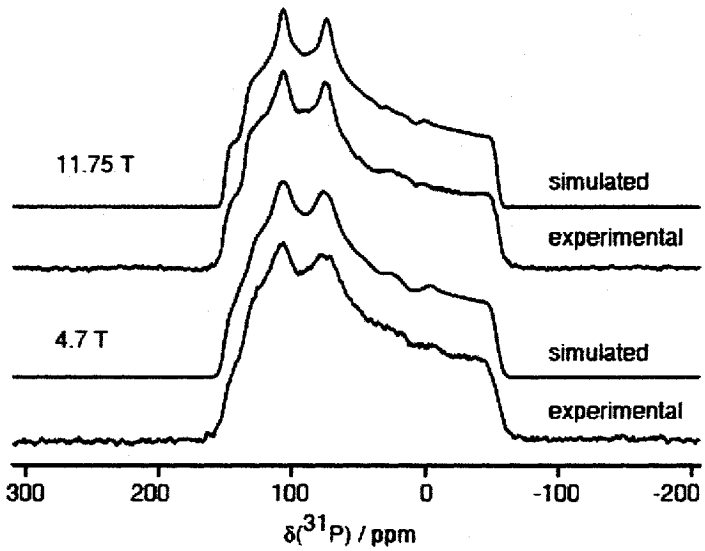

Figure 4.7 Solid-state $^{31}P\{^{1}H\}$ dipolar-chemical shift NMR spectra of **8c** obtained under stationary conditions.(11.75 T and 4.7 T). Simulated spectra produced using the parameters outlined in Table 4.2 and the WSOLIDS1 software package[33].

4.3.4. Two-Dimensional Solid State NMR

A series of two-dimensional correlation experiments was performed on **8c** to determine the through-bond connectivity of its two inequivalent ^{31}P nuclei. The off-diagonal peaks in the COSY spectrum (Figure 4.8a) and the correlations above and below the zero frequency axis (F_1 = 0) in the spin echo correlated spectroscopy (SECSY) spectrum (Figure 4.8b) indicated indirect nuclear spin-spin coupling.

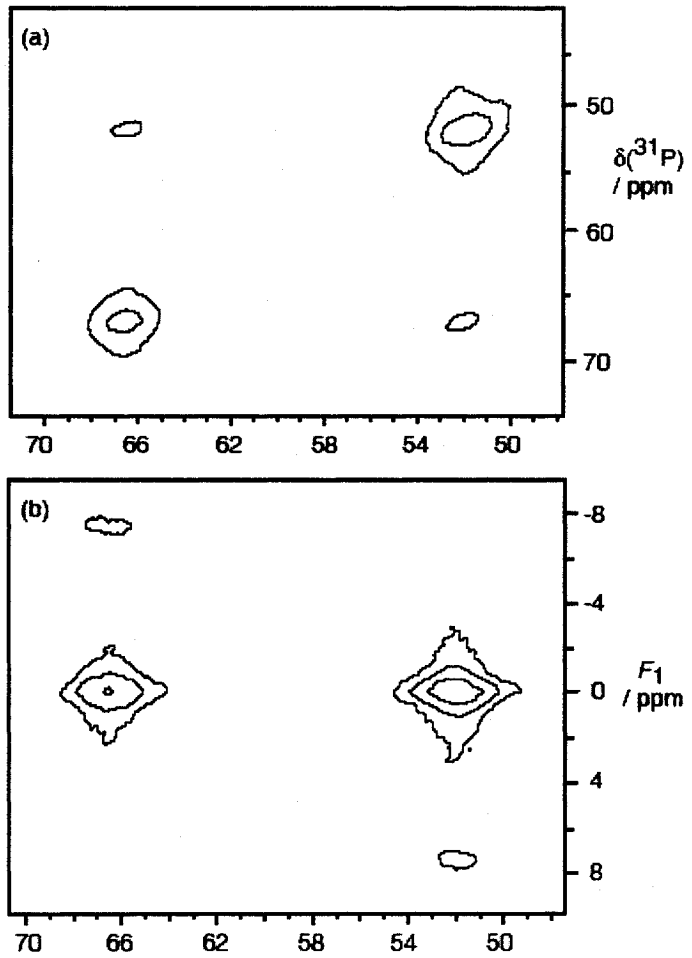

Figure 4.8 Solid-state NMR spectra of **8c** (4.7 T; MAS rate = 5.3 kHz). (a) ^{31}P-^{31}P CP/COSY. (b) ^{31}P CP/SECSY.

The 2D *J*-resolved spectrum,[34,35] which measures the indirect nuclear spin-spin coupling constants shows that the ^{31}P resonances arise from the same compound and not from different polymorphs in the same sample. Correlations are shown for the +1 spinning sideband (Figure 4.9). The magnitude of the *J* value in the F_1 dimension, $|^2J_{PP}| = 52 \pm 5$ Hz, is consistent with a *cis*-orientation of the phosphine ligands.[30] Solid state values for $|^2J_{PP}|$ for *cis*-disposed phosphine ligands are in good agreement with values seen in solution; in either case, values tend to be an

order of magnitude smaller than those for *trans*-disposed species. This is exemplified in the case of $RhCl(PPh_3)_3$, where $(^2J_{PP})_{cis} = 58 \pm 5$ Hz but $(^2J_{PP})_{trans} = 366$ Hz.[35]

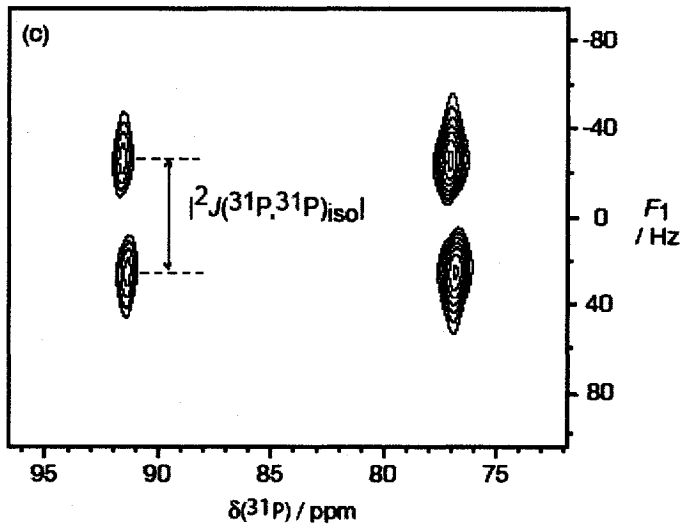

Figure 4.9 CP 2D *J*-resolved NMR spectrum (11.75 T; MAS rate = 5 kHz), showing the first-order spinning sidebands for each of the two inequivalent ^{31}P sites.

The data summarized below (Table 4.2) represent only the second set of ^{31}P chemical shift tensor magnitudes reported for an octahedral ruthenium complex. The first set was reported by Eichele and co-workers for $RuCl_2(\eta^1\text{-}Ph_2PCH_2CH_2OCH_3)_2(\eta^2\text{-en})$ in 2004. The values published for the principal components of the chemical shift tensor were δ_{11} = 95 to 109 ppm, δ_{22} = 56 to 76 ppm and δ_{33} = -75 to -60 ppm[36] for the five resolvable ^{31}P sites. The most striking difference that is found between the two data sets is reflected in the value of δ_{11}, where a difference in an order of magnitude is seen, as δ_{11} (**8**) equals 136.0 ppm and 149.8 ppm for sites A and B respectively.

Table 4.2 ^{31}P NMR parameters describing **8c** as determined from one- and two-dimensional ^{31}P solid-state NMR experiments.

	Site A	Site B
δ_{iso} [a] (ppm)	66.8 ± 0.5	52.1 ± 0.5
δ_{11} (ppm)	149.8 ± 1.0	136.0 ± 1.0
δ_{22} (ppm)	107.0 ± 1.0	75.0 ± 1.0
δ_{33} (ppm)	-55.0 ± 1.0	-53.5 ± 1.0
Ω (ppm)	205.5	189.5
κ	0.58	0.36
α [b] (°)	64 ±10	0 ± 10
β (°)	41 ± 10	-56 ± 10
γ (°)	35 ± 20	105 ± 20
$R_{eff\ (P\text{-}P)}$ (Hz)	660 ± 50	
$^2J_{(P\text{-}P)iso}$ (Hz)	52 ± 5	
$^1J_{(Ru\text{-}P)iso}$ (Hz)	244 ± 20	*c*
$d_{Ru\text{-}P}$ (Hz)	-140 ± 15	*d*

[a] Obtained from the 1D MAS NMR spectra. [b] The angles α, β, and γ define the orientations required to rotate the ^{31}P-^{31}P dipolar tensor into the chemical shift tensor principal axis system (PAS). The value of α for site B was arbitrarily set to zero since only the difference Δα affects the observed dipolar-chemical shift spectrum. [c] Splitting due to $J_{Ru\text{-}P}$ (where Ru = ^{99}Ru) is not as well resolved for site B; however the pattern is consistent with a coupling constant similar to that found for site A. [d] Splitting due to $J(^{99}Ru, ^{31}P)$ is not as well resolved for site B; however, the sense of the coupling pattern is opposite to that found for site A (figure 4.9), consistent with a significant difference in the orientation of the Ru-P dipolar vector relative to the ^{99}Ru electric field gradient principal axis system.

4.4. Determining Nuclearity of 8c by PGSE Diffusion NMR

The one and two-dimensional CP-MAS spectra, as well as the variable-temperature NMR experiment, described above, suggested that the triphenylphosphine ligands in **8** were *cis*-disposed, consistent with structure **8c**. MALDI-TOF mass spectrometry did not permit distinction between the mono and di-ruthenium possibilities (Figure 4.10). A signal corresponding to the monomeric structure $[RuCl(NN')(PPh_3)]^{+\bullet}$ (*m/z* Calc'd, 652.1; Found, 652.3) was observed; the base peak was $[Ru(NN')(PPh_3)]^{+\bullet}$ (*m/z* 615.5). Also present, however, were signals corresponding to a dinuclear (possibly agglomerated) species, though the intact dinuclear radial cation was not observed. The peak of highest *m/z* ratio corresponded to $[Ru_2Cl_2(NN')(PPh_3)_4]^{+\bullet}$ (*m/z* Calc'd, 1828.5; Found, 1044.2) and nothing of higher *m/z* was observed. In order to determine the nuclearity of **8** an NMR-based technique (PGSE NMR) was explored.

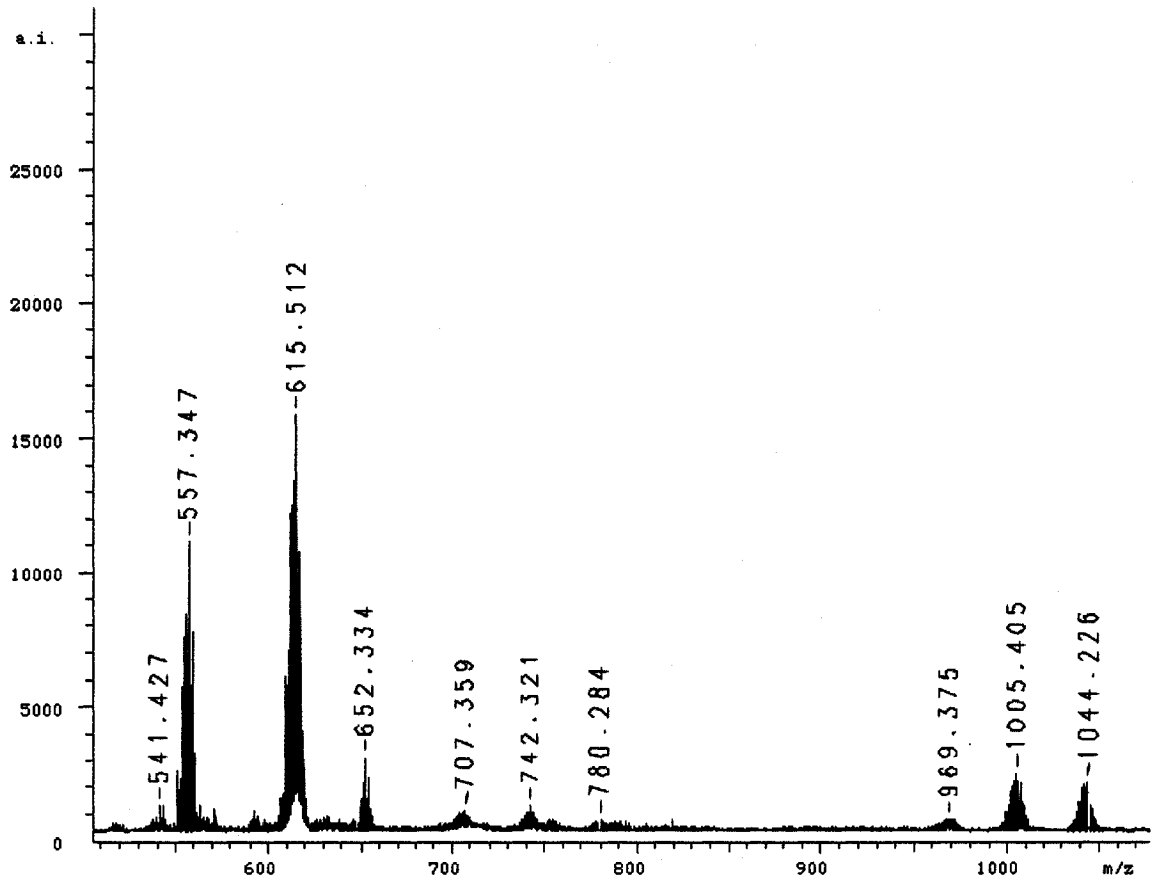

Figure 4.10 MALDI-TOF spectrum of **8**.

4.4.1. Theoretical Background and Governing Equations

The physical origin for translational diffusion relies upon the thermally-induced movement of molecules, or Brownian motion.[37] This form of diffusion occurs with no net external force acting on the system and leads to a random net displacement of the molecules over time. The rate of diffusion depends on the root mean square displacement of the molecules and their hydrodynamic radii, as well as the laminar flow of the sample.[37] Alternatively, the relative rate of diffusion can be described by a diffusion constant. The magnitude of the diffusion constant is proportional to the radius of the diffusing molecule and the viscosity of the medium through which the molecule is diffusing. Therefore, larger molecules in highly viscous media (i.e. at high concentrations) will have smaller diffusion constants than smaller molecules in more dilute media.

The first diffusion constant obtained by NMR methods came as a result of the discovery and monitoring of spin-echoes by Carl and Purcell,[38,39] and by Hahn[40] (Scheme 4.4). In the static spin echo (SE) experiment, a constant linear field gradient is applied in the direction of B_o. Nuclei at different spatial locations are labeled by different precessional frequencies (i.e. their magnetization become dephased). If the nuclei then diffuse through the sample, the phase they will acquire upon application of a refocusing pulse ($-\pi_y$) will be different from that acquired in the preparation step. The net consequence of applying the SE experiment to a sample containing diffusing molecules is an attenuation of the NMR signals corresponding to the partticular molecules relative to when no gradient is applied.

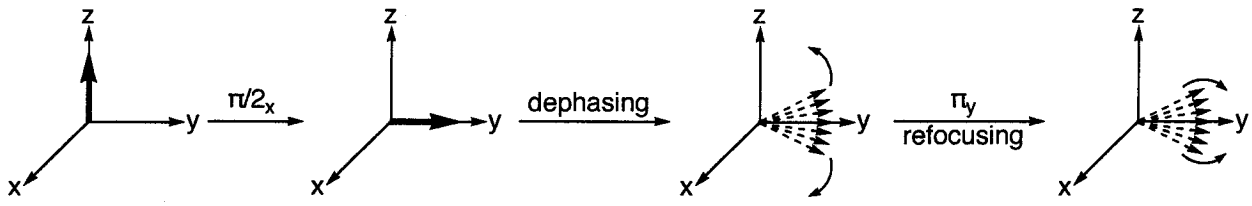

Scheme 4.4 The spin echo pulse sequence. The bolded arrow and the hashed arrows represent the magnetization vector of the sample.

The above technique, however, is no longer implemented due to methodological flaws. First, it is impossible to isolate the effects of diffusion from those due to transverse (T_2) relaxation; both of which cause signal attenuation.[37] Second, the constant application of increasingly stronger gradient amplitudes, to observe smaller diffusion constants, results in severe linewidth broadening. A corresponding shortening of the free induction decay following the first $(\pi/2)_x$ pulse and a decrease in the width of the echo following the second $(-\pi)_y$ pulse is also seen.[41]

By application of a pulsed field gradient instead of a static one, a discovery first made by M°Call[42] and later refined by Stejskal and Tanner,[41,43] these difficulties can be eliminated. The pulse sequence for the improved experiment (Scheme 4.5) still contains Hahn's echo sequence, which consists of a $(\pi/2)_x$ pulse followed by a $(-\pi)_y$ pulse. However, two gradient pulses are applied, rather than the constant gradient pulse used in the original experiment. The first gradient pulse is delivered after the initial $(\pi/2)_x$ pulse, and the second is applied after the $(-\pi)_y$ pulse. Both gradient pulses are equal in magnitude and the second gradient pulse is applied at a time interval (Δ, measured in milliseconds) from the first.

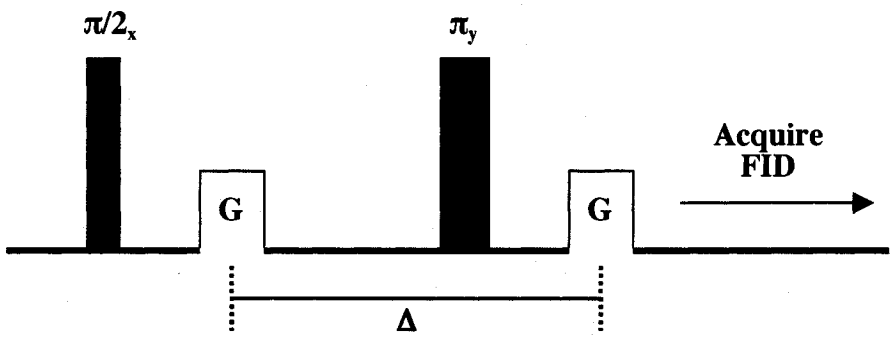

Scheme 4.5 The Stejskal-Tanner PGSE experiment.

The PGSE experiment is performed at a fixed RF pulse interval. Another experimental parameter, such as the interval between gradients (Δ), the gradient strength (G) or the gradient pulse duration (δ_G), is varied in order to keep the effects of T_2 relaxation constant. This permits the effects of T_2 relaxation to be distinguished from the attenuation in signal strength that results from diffusion.[37] Electronic requirements are also less demanding in the modified experiment, as observation of the echo is made in a homogeneous magnetic field (i.e. the gradients are off), and this eliminates the need for broadband circuitry.

In the present work, the PGSE experiment was performed by monitoring signal attenuation as a function of increased gradient strength (G). By plotting a graph of $\ln(I/I_0)$ versus the square of the gradient strength, a linear plot is generated. The slope of the resulting line is of the form y = mx + b, with b equal to zero and m equal to the "$-(\gamma\delta_G)^2(\Delta-\delta/3)$" portion of Equation 4.3.

$$\ln \frac{I}{I_0} = -(\gamma \delta_G)^2 G^2 \left(\Delta - \frac{\delta_G}{3}\right) D \qquad (4.3)$$

I = signal intensity at a given gradient strength, I_0 = signal intensity at 0 % gradient strength, γ = gyromagnetic ratio of nucleus under study (^{1}H = 26.7519 × 10^7 rad T^{-1} s^{-1}), δ_G = duration of gradient pulse (4 ms), G = gradient strength, Δ = delay between the midpoints of the gradients (10 ms), D = diffusion coefficient.

By plotting the results of PGSE measurements performed on several systems, one can differentiate between molecules of different sizes. Larger molecules, which diffuse more slowly will have smaller diffusion constants and this is reflected in lines with smaller slopes. Once the diffusion constant is known, the hydrodynamic radius (r_H) can be calculated from the Stokes-Einstein equation (Equation 4.4).

$$r_H = \frac{kT}{c\pi\eta D} \qquad (4.4)$$

r_H = hydrodynamic radius, k = Boltzmann's constant (1.381 × 10^{-23} J K^{-1}), T = temperature, η = viscosity parameter, D = diffusion constant.

When applying the Stokes-Einstein equation, corrections are usually made to the viscosity parameter, η, to account for temperature and concentration.[44] The viscosity parameter is typically measured at 298 K and without any solute. A rise in temperature would cause the viscosity of the solution and the value of the viscosity parameter to decrease, while an increase in solution concentration would cause an increase in both the solution viscosity and the viscosity parameter. If either of these effects is present in a PGSE experiment, and is left unaccounted for, the accuracy of the value for r_H would be low. An additional correction is made to the Stokes-Einstein equation for experiments at elevated concentrations. The value of the numerical factor,

c, must also be chosen correctly. The numerical factor represents the ratio of the hydrodynamic radius of the solvent to that of the solute. It accounts for the ease with which the molecules under study diffuse through the solvent. While this parameter can be determined exactly from microfriction theory,[45] it is valid to approximate the numerical factor to a general value based on the size of the diffusing species relative to the size of the solvent molecules. In our case, $c = 6$ and this represents a situation where the diffusing molecules are sufficiently larger than the solvent molecules surrounding it. This is also referred to as the "slip boundary condition".[45]

4.4.2. Diffusion Constant Determination for 8c

^{1}H-detected PGSE measurements were undertaken because the high sensitivity of the ^{1}H nucleus enables minimal experiment times and sample concentration, a function of the large gyromagnetic ratio and high magnetic susceptibility of the ^{1}H nucleus. Compound **8** was dissolved in $CDCl_3$ to give a sample concentration of 15 mM. An initial spectrum was obtained to determine the signal intensities at zero gradient strength (I_0). A series of 10 other spectra was measured at 10 % intervals of gradient strength, from 10 % to 100 %. As shown in Figure 4.11, using the pyrrole protons in **9a** as an example, as the gradient strength is increased all signals of are attenuated at approximately the same rate (observation of signal attenuations are different rates commonly indicates sample impurity).

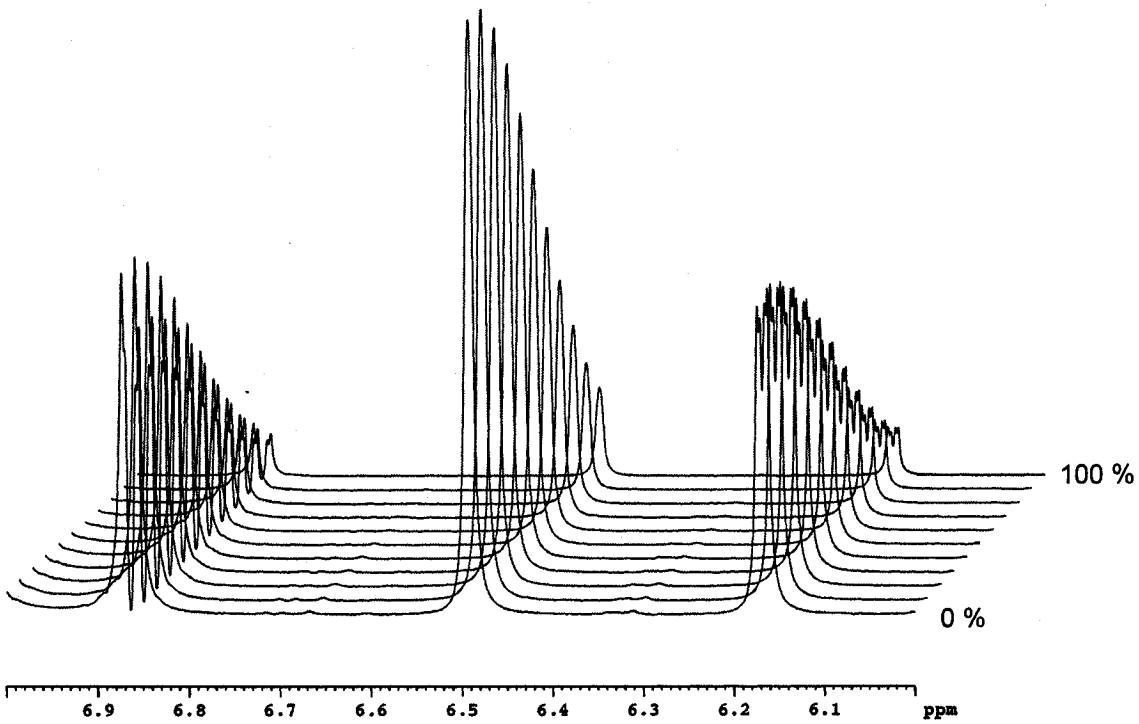

Figure 4.11 Signal attenuation of the pyrrole protons in **9a** as a function of increasing gradient strength (0 %-100 %).

Plots of $\ln(I/I_0)$ versus G^2 (Figure 4.13) are linear for **8**, **9** and **10**, consistent with Equation 4.3. Diffusion constants were extracted by solution of Equation 4.3 for each signal. By calculating an averaged value or "bulk diffusion constant", from the six most intense proton resonances in each spectrum, the impact of differing sensitivities and spin-relaxation effects for the individual protons can be minimized.

4.4.3. Nuclearity of 8c

In order to establish the nuclearity of **8**, the magnitude of its diffusion constant was compared to two reference compounds. Complexes **9a** and **10** were chosen to approximate the molecular volumes for the proposed monomeric and dimeric structures of **8**. The nuclearity of

9a has been previously established by X-ray diffraction. While no XRD data exists for **10**, data exists for the closely related dimeric species species $Ru_2Cl_5(dcypb)_2$.

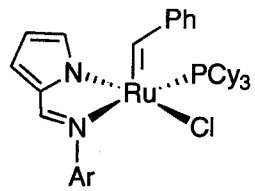

9a

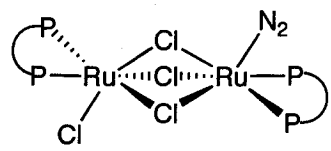

10

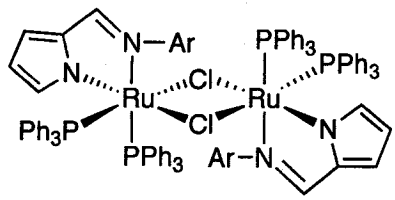

8c

Figure 4.12 Reference compounds **9a** and **10** and the proposed structure of **8** [Ar = 2,6-^{i}Pr-C_6H_3; PP = 1,4-bis(dicyclohexylphosphino)butane].

Figure 4.13 is a composite graph of $\ln(I/I_0)$ versus G^2, which was generated from data corresponding to the most intense signal in all three spectra (i.e. from spectra of **8c**, **9**, **10**). Consistent with the dimeric structure of **8c,** its diffusion constant is less than that for monomeric reference compound **9a** and dimeric reference compound **10**.

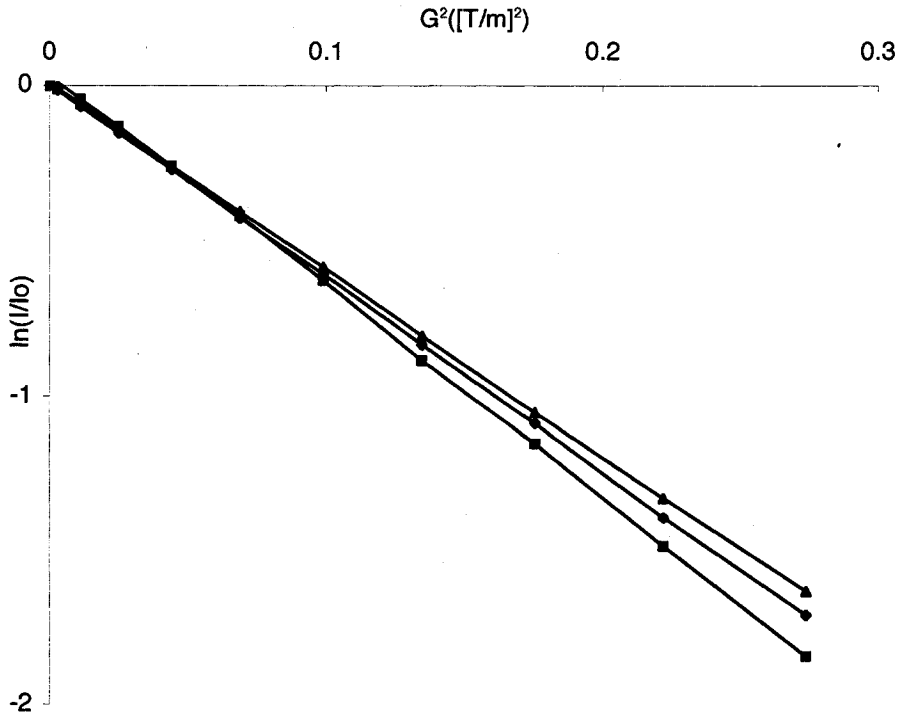

Figure 4.13 ^{1}H PGSE diffusion measurements for **8c** (▲) versus **10** (◆) and **9a** (■) ($CDCl_3$, 15 mM, 295 K). The slopes of the lines are related to the translational diffusion constants (see equation 4.3). Error bars for the lines are omitted for clarity and variance within a data set is expressed in terms of the standard deviation in *D* (see Table 4.3).

Table 4.3 Molecular weights, line slopes (from Figure 4.16) and diffusion constants (*D*) for **8c**, **9a**, **10**.

Complex	Molecular Weight (g mol^{-1})	Slope	*D* (10^{-10} m^2 s^{-1})	Standard Deviation in *D* (10^{-10} m^2 s^{-1})
9a	842.40	-6.8064	6.86	0.0255
10	1273.78	-6.2483	6.30	0.0615
8c	1828.62	-5.9982	6.04	0.0501

To evaluate the accuracy of these diffusion constants, the hydrodynamic radii of **8c**, **9a** and **10** were calculated by solution of Equation 4.4 and then compared to known radii derived from X-ray crystallographic structures (r_{XRD}). Under optimal conditions, including when experiments are performed in non-coordinating solvent with no potential for hydrogen-bonding, the agreement between the two values can be within a 0.01 Å.[46] In solving the Stokes-Einstein equation (Equation 4.4), solution viscosity was approximated with solvent viscosity (i.e. variable η) and this results in an under-estimation of η. By choosing the approximated numerical factor corresponding to the slip boundary condition (i.e. $c = 6$), an over-estimation in c occurs. The combination of an under-estimation in η and an over-estimation in c results in an error in the final value of r_H of less than 5 %.[45]

Table 4.4 Comparison of hydrodynamic radii obtained from PGSE experiments versus the radii obtained from crystallographic data.

Compound	r_H (Å)	r_{XRD} (Å)	Ref
8c	7.00	N/A	This work
9a	6.15	6.10	2
10	6.70	6.92[a]	47
$ZrCl_2(Cp)_2$	3.0	3.1	46
$[Ru_2(\mu\text{-}Cl_3)(mesetph)_2]Cl$[b]	7.8	7.5	46

[a]Radius for $Ru_2Cl_5(dcypb)_2$ is substituted for **10**, which lacks an x-ray structure. [b]Where mesetph is $MesP\{CH_2CH_2P(C_6H_5)_2\}_2$.

The agreement between r_H and r_{XRD} is acceptable when compared to the literature precedent (Table 4.4), suggesting that the assumptions made to solve the Stokes-Einstein

equation (*vide supra*) were valid. Further evidence for the dimeric nature of **8c** is also presented in this table, as its radius is larger than that observed for dimeric **10**. The difference in r_H for monomeric **9a** and dimeric **10** is only 0.55 Å. The small size of this difference highlights the importance of choosing reference compounds that correspond as close as possible to the upper and lower limits for the proposed diffusion constant of an unknown compound.

4.5. Conclusions

This chapter describes the formation of a stable, N, N'-chelated iminopyrrolato ligand within an edge-bridged ruthenium dimer containing *cis*-disposed triphenylphosphine ligands. The resistance of **8c** to $\sigma \rightarrow \pi$ isomerization, despite the ease with which a vacant site could be created via loss of a triphenylphosphine or a datively-bound chloride, suggests that the σ-pyrrolide donor is stable within the five-membered chelate ring. A PGSE NMR study established the dimeric structure of **8c** by comparison of its diffusion constant to those of appropriately chosen reference compounds. Further investigation of catalysts containing related pyrrolide-based pseudohalide ligands is of interest, with their application to olefin metathesis a goal. Solid-state NMR experiments proved invaluable in revealing the unexpected *cis*-disposition of the two triphenylphosphine ligands in complex **8**. During the course of this work, the largest ever ruthenium-phosphorus spin-spin coupling constant was measured and only the second set of ^{31}P chemical shift tensor magnitudes for an octahedral ruthenium complex were reported.

4.6 References

(1) (a) Conrad, J. C.; Parnas, H. H.; Snelgrove, J. L.; Fogg, D. E. *J. Amer. Chem. Soc.* **2005**, *127*, 11882. (b) Conrad, J. C.; Amoroso, D.; Czechura, P.; Yap, G. P. A.; Fogg, D. E. *Organometallics* **2003**, *22*, 3634. (c) Conrad, J. C.; Fogg, D. E. *Curr. Org. Chem.* **2006**, *10*, 185, and references therein.

(2) Drouin, S. D.; Foucault, H. M.; Yap, G. P. A.; Fogg, D. E. *Can. J. Chem.* **2005**, *83*, 748.

(3) Kershner, D. L.; Basolo, F. *Coord. Chem. Rev.* **1987**, *19*, 279.

(4) DuBois, M. R. *Coord. Chem. Rev.* **1998**, *174*, 191.

(5) Sadimenko, A. P.; Garnovskii, A. D.; Retta, N. *Coord. Chem. Rev.* **1993**, *126*, 237.

(6) DuBois, M. R.; Parker, K. G.; Ohman, C.; Noll, B. C. *Organometallics* **1997**, *16*, 2325.

(7) Dawson, D. M.; Walker, D. A.; Thornton-Pett, M.; Bochmann, M. *J. Chem. Soc., Dalton Trans.* **2000**, 459.

(8) Hao, H.; Bhandari, S.; Ding, Y.; Roesky, H. W.; Magull, J.; Schmidt, H.-G.; Noltemeyer, M.; Cui, C. *Eur. J. Inorg. Chem.* **2002**, 1060.

(9) Yoshida, Y.; Saito, J.; Mitani, M.; Takagi, Y.; Matsui, S.; Ishii, S.-I.; Nakano, T.; Kashiwa, N.; Fujita, T. *Chem. Commun.* **2002**, 1298.

(10) Matsuo, Y.; Mashima, K.; Tani, K. *Organometallics* **2001**, *20*, 3510.

(11) Yoshida, Y.; Matsui, S.; Takagi, Y.; Mitani, M.; Nakano, T.; Tanaka, H.; Kashiwa, N.; Fujita, T. *Organometallics* **2001**, *20*, 4793.

(12) Sasabe, H.; Nakanishi, S.; Takata, T. *Inorg. Chem. Commun.* **2003**, *6*, 1140.

(13) Snelgrove, J. L.; Conrad, J. C.; Eelman, M. D.; Moriarty, M. M.; Yap, G. P. A.; Fogg, D. E. *Organometallics* **2005**, *24*, 103.

(14) Monfette, S.; Fogg, D. E. *Organometallics* **2006**, *25*, 1940.

(15) Matsuo, Y.; Mashima, K.; Tani, K. *Chem. Lett.* **2000**, 1114.

(16) Laws, D. D.; Bitter, H.-M. L.; Jerschow, A. *Angew. Chem. Int. Ed.* **2002**, *41*, 3096.

(17) Lambert, J. B.; Shurvell, H. F.; Lightner, D. A.; Cooks, R. G. *Organic Structural Spectroscopy*, 1998, p. 568.

(18) Stejskal, E. O.; Memory, J. D. *High Resolution NMR in the Solid State: Fundamentals of CP/MAS*, Oxford University Press: New York, NY, 1994, p. 189.

(19) Bemi, L.; Clark, H. C.; Davies, J. A.; Fyfe, C. A.; Wasylishen, R. E. *J. Am. Chem. Soc.* **1982**, *104*, 438.

(20) Andrew, E. R.; Bradbury, A.; Eades, R. G. *Nature* **1958**, *182*, 1659.

(21) Lowe, I. J. *Phys. Rev. Lett.* **1959**, *2*, 285.

(22) Weast, R. C.; Selby, S. M. *Handbook of Chemistry and Physics, 55th Ed*, 1974.

(23) Grant, D. M.; Harris, R. K.; Editors *Encyclopedia of Nuclear Magnetic Resonance, Volume 9: Advances in NMR*, 2002.

(24) Pines, A.; Gibby, M. G.; Waugh, J. S. *J. Chem. Phys.* **1972**, *56*, 1776.

(25) Pines, A.; Gibby, M. G.; Waugh, J. S. *Chem. Phys. Lett.* **1972**, *15*, 373.

(26) Pines, A.; Gibby, M. G.; Waugh, J. S. *J. Chem. Phys.* **1973**, *59*, 569.

(27) Hartmann, S. R.; Hahn, E. L. *Phys. Rev.* **1962**, *128*, 2042.

(28) Rosman, K. J. R.; Taylor, P. D. P. *Pure Appl. Chem.* **1998**, *70*, 217.

(29) Eichele, K.; Wasylishen, R. E.; Corrigan, J. F.; Doherty, S.; Carty, A. J.; Sun, Y. *Inorg. Chem.* **1993**, *32*, 121.

(30) Verkade, J. G.; Quin, L. D., Ed. *Methods in Stereochemical Analysis: Phosphorus-31 NMR Spectroscopy in Stereochemical Analysis*. VCH: Deerfield Beach, Fla, 1987.

(31) (a) VanderHart, D. L.; Gutowsky, H. S. *J. Chem. Phys.* **1968**, *49*, 261. (b) VanderHart, D. L.; Gutowsky, H. S.; Farrar, T. C. *J. Chem. Phys.* **1969**, *50*, 1058. (c) Linder, M.; Hoehener, A.; Ernst, R. R. *J. Chem. Phys.* **1980**, *73*, 4959. (d) Eichele, K.; Wasylishen, R. E. *J. Magn. Reson. A* **1994**, *106*, 46.

(32) La Placa, S. J.; Ibers, J. A. *Inorg. Chem.* **1965**, *4*, 778.

(33) Eichele, K., Wasylishen, R. E. *WSOLIDS NMR Simulation Package*, 1.17.30; Dalhousie University: Halifax, 2001.

(34) Wu, G.; Wasylishen, R. E.; Curtis, R. D. *Can. J. Chem.* **1992**, *70*, 863.

(35) Wu, G.; Wasylishen, R. E. *Inorg. Chem.* **1992**, *31*, 145.

(36) Wu, G.; Wasylishen, R. E. *Organometallics* **1992**, *11*, 3242.

(37) Stilbs, P. *Prog. Nucl. Magn. Reson. Spectrosc.* **1987**, *19*, 1.

(38) Carr, H. Y.; Purcell, E. M. *Phys. Rev.* **1954**, *94*, 630.

(39) Woessner, D. E. *J. Chem. Phys.* **1961**, *34*, 2057.

(40) Hahn, E. L. *Phys. Rev.* **1950**, *80*, 580.

(41) Stejskal, E. O.; Tanner, J. E. *J. Chem. Phys.* **1965**, *42*, 288.

(42) McCall, D. W.; Douglass, D. C.; Anderson, E. W. *Ber. Bunsen-Ges. Phys. Chem* **1963**, *67*, 336.

(43) Boss, B. D.; Stejskal, E. O.; Ferry, J. D. *J. Phys. Chem.* **1967**, *71*, 1501.

(44) Edward, J. T. *J. Chem. Educ.* **1970**, *47*, 261.

(45) Zuccaccia, D.; Macchioni, A. *Organometallics* **2005**, *24*, 3476.

(46) Pregosin, P. S.; Kumar, P. G. A.; Fernandez, I. *Chem. Rev.* **2005**, *105*, 2977.

(47) Amoroso, D.; Yap, G. P. A.; Fogg, D. E. *Can. J. Chem.* **2001**, *79*, 958.

CHAPTER 5

Conclusions and Recommendations for Future Work

The work summarized in this thesis illustrates the utility of neutral two-electron donor ligands, including π-acids and nitrogen heterocycles, as both phosphine replacements and components of pseudohalide ligands. In Chapter 3, novel ruthenium hydrogenation catalysts $RuHCl(CO)(IMes)(PPh_3)$ and $RuHCl(CO)(H_2IMes)(PPh_3)$ were shown to exhibit superior activity for the hydrogenation of internal and unactivated olefins, relative to known catalysts $RuHCl(CO)(NHC)(PCy_3)$ and $RuHCl(CO)(PCy_3)_2$. The increased lability of PPh_3, relative to PCy_3, was determined to be essential for the activating effect of the carbene to be seen. NMR studies involving ^{31}P inversion transfer experiments are currently underway in this laboratory in order to determine the extent of this effect. Future work will include substitution of phosphine for pyridine, which would reduce π-acidity trans to the *N*-heterocyclic carbene and create a weaker metal-pyridine bond. Incorporation of a chiral *N*-heterocyclic carbene, paralleling the trend in development of catalysts for asymmetric hydrogenation, is also an area of future interest.

Additional work in Chapter 3 included a computational analysis of ethene reduction by model systems $RuHCl(CO)(PH_3)_2$ and $RuHCl(PH_3)_3$. Data could not be found to support the proposal that the incorporation of a carbonyl ligand into a ruthenium hydride catalyst activates it for hydrogenation. Substitution of CO for PH_3, generating $RuHCl(CO)(PH_3)_2$, did not cause a favourable change in mechanism nor did it stabilize the rate-limiting step of the reaction. If the carbonyl ligand is activating for ruthenium-catalyzed hydrogenation it may result from the ability of this ligand to stabilize the active catalyst towards olefin coordination or towards decomposition to an extent that a labile donor, such as H_2, cannot. Future work involving

computational analysis of systems containing more relevant phosphines (i.e. PCy_3 and PPh_3), will permit a more direct link to experimental data.

In Chapter 4, the resistance to $\sigma \rightarrow \pi$ isomzerization afforded by a chelating iminopyrrolato ligand was examined through synthesis of $RuCl(\kappa^2\text{-}N,N'\text{-}(2,6\text{-}^{i}Pr_2C_6H_3)\text{-}N{=}CHC_4H_3N)(PPh_3)_2]_2$ (**8**). Detailed one and two-dimensional solution state NMR experiments confirmed retention of the σ-binding mode and pulsed field gradient spin-echo (PGSE) diffusion NMR measurements permitted distinction between mononuclear **8a** and dinuclear **8b/8c.** Two-dimensional COSY, SECSY, and *J*-resolved solid-state ^{31}P NMR experiments confirm that the PPh_3 ligands on each metal center are *cis*-disposed, implying **8c**. Future work will include design of complexes containing highly labile ligands with greater relevance to olefin metathesis, now that the stability of the iminopyrrolide against π-coordination has been established. Incorporation of electron-withdrawing groups or chiral substituents on the iminopyrrolide ligand would broaden its applicability and are possibilities for further investigation.